Williams, Alan N., Ulm, Sean, Sapienza, Tom, Lewis, Stephen, and Turney, Chris S.M. (2018) *Sea-level change and demography during the last glacial termination and early Holocene across the Australian continent.* Quaternary Science Reviews, 182. pp. 144-154.

http://dx.doi.org/ 10.1016/j.quascirev.2017.11.030

Supplementary Information

The following sections provide further information on the methods used in this study. Here we reproduce extracts of Williams (2013), Williams et al. (2013, 2015) and Lewis et al. (2013) from where many of the methods were adopted, and elaborate on new methods employed in this study.

Sea-level

Developing a sea-level curve

To determine the timing and extent of sea-level change, we used the line-of-best fit through a combined dataset of Lewis et al. (2013) and Lambeck et al. (2002) (see also Yokoyama et al., 2001a, 2001b) (Figure S1). These values generally took the midpoint of data within the envelope developed at any given time interval to provide a single value with which to explore changing continental landmass. Specific sea-level values determined from this approach are presented in Table S1.

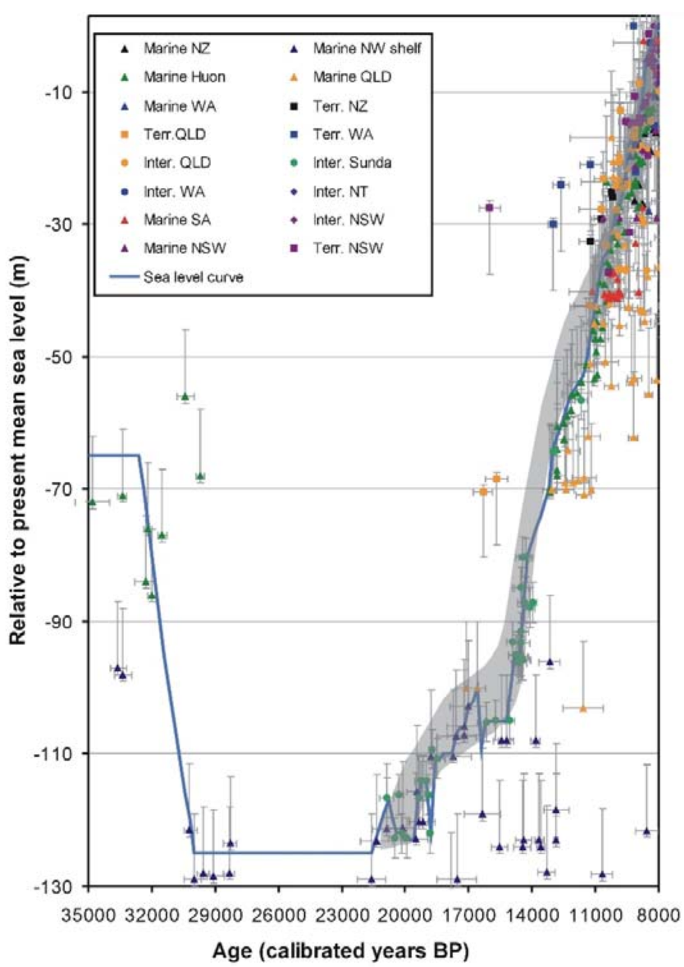

Figure S1: Sea-level data from Lewis et al. (2013) showing the line of best fit use for this analysis.

Table S1: Sea-level data (metres below PMSL) used in this analysis.

Age (ka)	Metres PMSL	Age (ka)	Metres PMSL	Age (ka)	Metres PMSL	Age (ka)	Metres PMSL
8000	0	16800	-101.5	25600	-125	34400	-65
8200	-2	17000	-103	25800	-125	34600	-65
8400	-3	17200	-106	26000	-125	34800	-65
8600	-6	17400	-106	26200	-125	35000	-65
8800	-12	17600	-107	26400	-125		
9000	-14	17800	-110	26600	-125		
9200	-16	18000	-110	26800	-125		
9400	-18	18200	-110	27000	-125		
9600	-24	18400	-111	27200	-125		
9800	-27	18600	-111	27400	-125		
10000	-28	18800	-122	27600	-125		
10200	-31	19000	-114	27800	-125		
10400	-34	19200	-114	28000	-125		
10600	-35	19400	-117	28200	-125		
10800	-38	19600	-123	28400	-125		
11000	-42	19800	-123	28600	-125		
11200	-46	20000	-123	28800	-125		
11400	-50	20200	-122	29000	-125		
11600	-53	20400	-122	29200	-125		
11800	-54	20600	-119.5	29400	-125		
12000	-55	20800	-117	29600	-125		
12200	-56	21000	-119	29800	-125		
12400	-58	21200	-121	30000	-125		
12600	-60	21400	-123	30200	-120		
12800	-62	21600	-125	30400	-116		
13000	-64	21800	-125	30600	-112		
13200	-70	22000	-125	30800	-108		
13400	-72	22200	-125	31000	-104		
13600	-74	22400	-125	31200	-100		
13800	-76	22600	-125	31400	-95		
14000	-78	22800	-125	31600	-90		
14200	-80	23000	-125	31800	-85		
14400	-87	23200	-125	32000	-80		
14600	-96	23400	-125	32200	-75		
14800	-95	23600	-125	32400	-70		
15000	-100	23800	-125	32600	-65		
15200	-105	24000	-125	32800	-65		
15400	-105	24200	-125	33000	-65		
15600	-105	24400	-125	33200	-65		
15800	-105	24600	-125	33400	-65		
16000	-105	24800	-125	33600	-65		
16200	-105	25000	-125	33800	-65		
16400	-109	25200	-125	34000	-65		
16600	-100	25400	-125	34200	-65		

Changing Land Mass

As outlined in the manuscript, we used GIS analysis of bathymetric data at given time intervals to identify the amount of crustal shelf gained or lost. A summary of the changes is provided in the manuscript, with the complete record at 200 year intervals presented in Table S2.

Table S2: Changing continental landmass, sea-level, Aboriginal populations and density for selected time periods. Aboriginal populations are based on data in Williams (2013) (uncorrected radiocarbon data; founding population of 2,500 at 50 ka; and a smoothing spline with 50 degrees of freedom).

Date (ka)	**Relative Sea-level (m PMSL)**	**Continental Landmass (km^2)**	**Change from previous presented time interval (km^2)**	**Change from previous presented time interval (%)**	**Population (*n*)**	**Population (1/ n km^2)**
35,000	-65	9,113,772	0.00	0.00	13,922.39	655
34,800	-65	9,113,772	0.00	0.00	13,313.22	685
34,600	-65	9,113,772	0.00	0.00	12,855.12	709
34,400	-65	9,113,772	0.00	0.00	12,388.69	736
34,200	-65	9,113,772	0.00	0.00	11,762.25	775
34,000	-65	9,113,772	0.00	0.00	10,999.91	829
33,800	-65	9,113,772	0.00	0.00	10,297.73	885
33,600	-65	9,113,772	0.00	0.00	9,861.10	924
33,400	-65	9,113,772	0.00	0.00	9,758.44	934
33,200	-65	9,113,772	0.00	0.00	9,915.19	919
33,000	-65	9,113,772	0.00	0.00	10,239.46	890
32,800	-65	9,113,772	0.00	0.00	10,654.26	855
32,600	-65	9,113,772	0.00	0.00	11,111.53	820
32,400	-70	9,241,439	127,666.40	1.40	11,698.73	790
32,200	-75	9,327,152	85,712.95	0.93	12,606.92	740
32,000	-80	9,412,929	85,776.93	0.92	13,868.83	679
31,800	-85	9,480,088	67,159.15	0.71	15,320.73	619
31,600	-90	9,537,990	57,902.21	0.61	16,714.30	571
31,400	-95	9,591,060	53,070.52	0.56	17,611.58	545
31,200	-100	9,638,459	47,398.91	0.49	17,538.21	550
31,000	-104	9,672,960	34,500.81	0.36	16,590.43	583
30,800	-108	9,701,229	28,269.30	0.29	15,403.03	630
30,600	-112	9,727,288	26,058.83	0.27	14,604.17	666
30,400	-116	9,751,396	24,107.85	0.25	14,375.77	678
30,200	-120	9,773,718	22,322.13	0.23	14,432.30	677
30,000	-125	9,799,737	26,018.26	0.27	14,422.20	679
29,800	-125	9,799,737	0.00	0.00	14,221.49	689
29,600	-125	9,799,737	0.00	0.00	13,919.19	704
29,400	-125	9,799,737	0.00	0.00	13,564.17	722

Date (ka)	Relative Sea-level (m PMSL)	Continental Landmass (km^2)	Change from previous presented time interval (km^2)	Change from previous presented time interval (%)	Population (*n*)	Population (1/ *n* km^2)
29,200	-125	9,799,737	0.00	0.00	13,121.54	747
29,000	-125	9,799,737	0.00	0.00	12,593.48	778
28,800	-125	9,799,737	0.00	0.00	12,250.71	800
28,600	-125	9,799,737	0.00	0.00	12,560.15	780
28,400	-125	9,799,737	0.00	0.00	13,568.41	722
28,200	-125	9,799,737	0.00	0.00	14,790.66	663
28,000	-125	9,799,737	0.00	0.00	15,687.34	625
27,800	-125	9,799,737	0.00	0.00	16,081.07	609
27,600	-125	9,799,737	0.00	0.00	16,133.50	607
27,400	-125	9,799,737	0.00	0.00	16,015.59	612
27,200	-125	9,799,737	0.00	0.00	15,844.77	618
27,000	-125	9,799,737	0.00	0.00	15,695.39	624
26,800	-125	9,799,737	0.00	0.00	15,481.13	633
26,600	-125	9,799,737	0.00	0.00	15,004.06	653
26,400	-125	9,799,737	0.00	0.00	14,262.52	687
26,200	-125	9,799,737	0.00	0.00	13,474.73	727
26,000	-125	9,799,737	0.00	0.00	12,881.65	761
25,800	-125	9,799,737	0.00	0.00	12,632.63	776
25,600	-125	9,799,737	0.00	0.00	12,785.43	766
25,400	-125	9,799,737	0.00	0.00	13,318.73	736
25,200	-125	9,799,737	0.00	0.00	13,896.87	705
25,000	-125	9,799,737	0.00	0.00	13,992.54	700
24,800	-125	9,799,737	0.00	0.00	13,571.92	722
24,600	-125	9,799,737	0.00	0.00	13,123.49	747
24,400	-125	9,799,737	0.00	0.00	13,174.97	744
24,200	-125	9,799,737	0.00	0.00	13,947.94	703
24,000	-125	9,799,737	0.00	0.00	15,310.92	640
23,800	-125	9,799,737	0.00	0.00	16,954.93	578
23,600	-125	9,799,737	0.00	0.00	18,473.36	530
23,400	-125	9,799,737	0.00	0.00	19,548.11	501
23,200	-125	9,799,737	0.00	0.00	20,351.43	482
23,000	-125	9,799,737	0.00	0.00	21,443.48	457
22,800	-125	9,799,737	0.00	0.00	23,023.62	426
22,600	-125	9,799,737	0.00	0.00	24,826.61	395
22,400	-125	9,799,737	0.00	0.00	26,484.88	370
22,200	-125	9,799,737	0.00	0.00	27,624.63	355
22,000	-125	9,799,737	0.00	0.00	27,932.12	351
21,800	-125	9,799,737	0.00	0.00	27,372.45	358
21,600	-125	9,799,737	0.00	0.00	26,169.58	374
21,400	-123	9,789,429	-10,307.23	-0.11	24,590.29	398

Date (ka)	Relative Sea-level (m PMSL)	Continental Landmass (km^2)	Change from previous presented time interval (km^2)	Change from previous presented time interval (%)	Population (*n*)	Population (1/ *n* km^2)
21,200	-121	9,778,959	-10,470.00	-0.11	22,922.75	427
21,000	-119	9,768,281	-10,678.56	-0.11	21,484.69	455
20,800	-117	9,757,184	-11,096.56	-0.11	20,584.69	474
20,600	-120	9,773,718	16,534.09	0.17	20,423.21	479
20,400	-122	9,784,197	10,478.93	0.11	21,149.51	463
20,200	-122	9,784,197	0.00	0.00	23,229.18	421
20,000	-123	9,789,429	5,232.11	0.05	27,540.38	355
19,800	-123	9,789,429	0.00	0.00	34,795.99	281
19,600	-123	9,789,429	0.00	0.00	43,832.22	223
19,400	-117	9,757,184	-32,245.12	-0.33	51,790.98	188
19,200	-114	9,739,302	-17,881.75	-0.18	56,767.96	172
19,000	-114	9,739,302	0.00	0.00	58,204.03	167
18,800	-122	9,784,197	44,894.76	0.46	56,056.70	175
18,600	-111	9,720,946	-63,251.21	-0.65	51,337.03	189
18,400	-111	9,720,946	0.00	0.00	45,817.67	212
18,200	-110	9,714,493	-6,453.44	-0.07	40,543.12	240
18,000	-110	9,714,493	0.00	0.00	35,712.73	272
17,800	-110	9,714,493	0.00	0.00	31,381.18	310
17,600	-107	9,694,370	-20,122.23	-0.21	27,702.01	350
17,400	-106	9,687,522	-6,848.81	-0.07	24,920.43	389
17,200	-106	9,687,522	0.00	0.00	23,237.56	417
17,000	-103	9,665,164	-22,357.09	-0.23	22,791.09	424
16,800	-102	9,656,831	-8,333.28	-0.09	23,685.78	408
16,600	-100	9,638,459	-18,371.79	-0.19	25,851.30	373
16,400	-109	9,707,821	69,361.58	0.72	29,010.41	335
16,200	-105	9,680,365	-27,455.83	-0.28	32,649.16	296
16,000	-105	9,680,365	0.00	0.00	35,444.77	273
15,800	-105	9,680,365	0.00	0.00	35,764.22	271
15,600	-105	9,680,365	0.00	0.00	33,665.67	288
15,400	-105	9,680,365	0.00	0.00	30,792.04	314
15,200	-105	9,680,365	0.00	0.00	28,827.40	336
15,000	-100	9,638,459	-41,905.74	-0.43	28,629.66	337
14,800	-95	9,591,060	-47,398.91	-0.49	30,094.07	319
14,600	-96	9,601,093	10,032.21	0.10	32,303.07	297
14,400	-87	9,503,745	-97,347.34	-1.01	33,723.75	282
14,200	-80	9,412,929	-90,816.74	-0.96	33,083.76	285
14,000	-78	9,380,670	-32,258.96	-0.34	30,576.16	307
13,800	-76	9,345,575	-35,094.68	-0.37	27,559.33	339
13,600	-74	9,308,409	-37,165.77	-0.40	25,012.05	372
13,400	-72	9,274,597	-33,811.71	-0.36	23,367.13	397

Date (ka)	Relative Sea-level (m PMSL)	Continental Landmass (km²)	Change from previous presented time interval (km²)	Change from previous presented time interval (%)	Population (*n*)	Population (1/ *n* km²)
13,200	-70	9,241,439	-33,158.75	-0.36	22,928.25	403
13,000	-64	9,079,658	-161,781.01	-1.75	23,731.70	383
12,800	-62	9,015,755	-63,902.46	-0.70	25,496.14	354
12,600	-60	8,951,490	-64,265.14	-0.71	27,858.48	321
12,400	-58	8,878,702	-72,787.62	-0.81	30,534.79	291
12,200	-56	8,796,978	-81,724.81	-0.92	33,315.52	264
12,000	-55	8,754,285	-42,692.17	-0.49	35,904.24	244
11,800	-54	8,718,718	-35,567.24	-0.41	37,905.16	230
11,600	-53	8,688,353	-30,365.67	-0.35	39,123.81	222
11,400	-50	8,614,163	-74,189.37	-0.85	40,401.02	213
11,200	-46	8,521,759	-92,404.32	-1.07	43,303.11	197
11,000	-42	8,436,419	-85,340.10	-1.00	47,874.45	176
10,800	-38	8,362,487	-73,932.07	-0.88	52,327.88	160
10,600	-35	8,310,729	-51,757.66	-0.62	54,866.54	151
10,400	-34	8,294,144	-16,585.36	-0.20	55,412.60	150
10,200	-31	8,244,144	-50,000.14	-0.60	55,367.08	149
10,000	-28	8,190,877	-53,266.53	-0.65	55,810.30	147
9,800	-27	8,173,931	-16,946.11	-0.21	57,238.68	143
9,600	-24	8,121,137	-52,793.95	-0.65	59,906.99	136
9,400	-18	8,013,754	-107,383.21	-1.32	63,363.01	126
9,200	-16	7,981,573	-32,180.86	-0.40	66,673.50	120
9,000	-14	7,952,360	-29,212.84	-0.37	69,967.82	114
8,800	-12	7,922,133	-30,227.52	-0.38	74,603.18	106
8,600	-6	7,839,223	-82,909.06	-1.05	81,892.00	96
8,400	-3	7,794,815	-44,408.91	-0.57	91,396.86	85
8,200	-2	7,778,369	-16,445.44	-0.21	100,842.20	77
8,000	0	7,684,306	-94,062.72	-1.21	107,936.79	71
Average		*9,392,435*	*-10,510.78*	*-0.12*	*28,148.6*	*467.9*
Total			**-142,9465.88**	**-16.93**		

Analysis of Shore-line change

To determine the pace of sea-level change, we adopted methods from Anderson and Bissett (2015). Specifically, we measured a series of transects distributed across Australia (Figures S2-S20), and encompassing the crustal shelf. The transects were selected to provide a broad spread across the continent. We then measured the distances of the changing coastline along each transect during the selected time intervals. The data recovered from this process are presented in Table S3, with the summary information developed from these transects presented in Table 2.

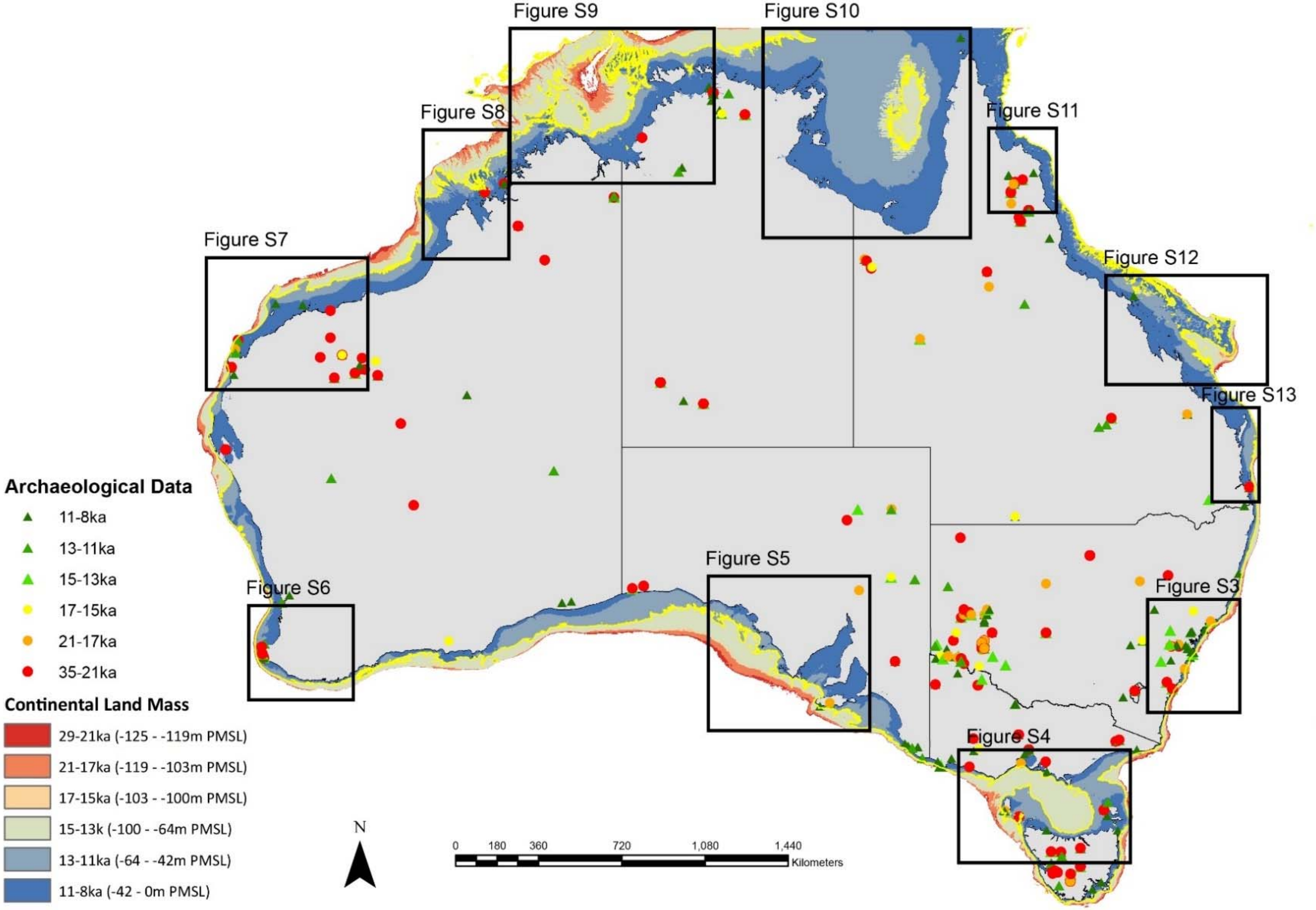

Figure S2: Overall location map of sea-level transect data presented in Figures S3-S13 inclusive.

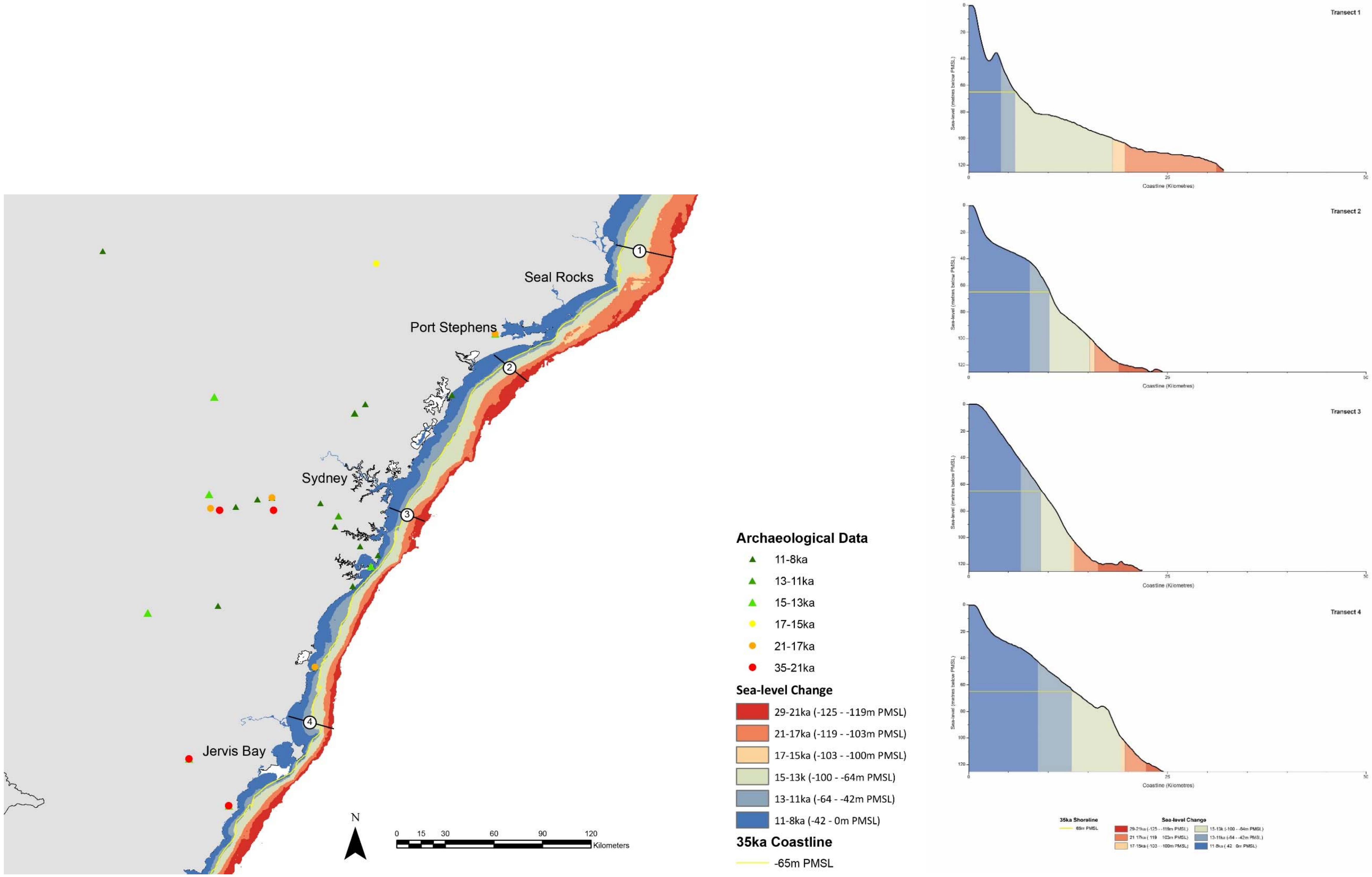

Figure S3: Sea-level transects and cross sections 1-4 inclusive, located along the NSW coast.

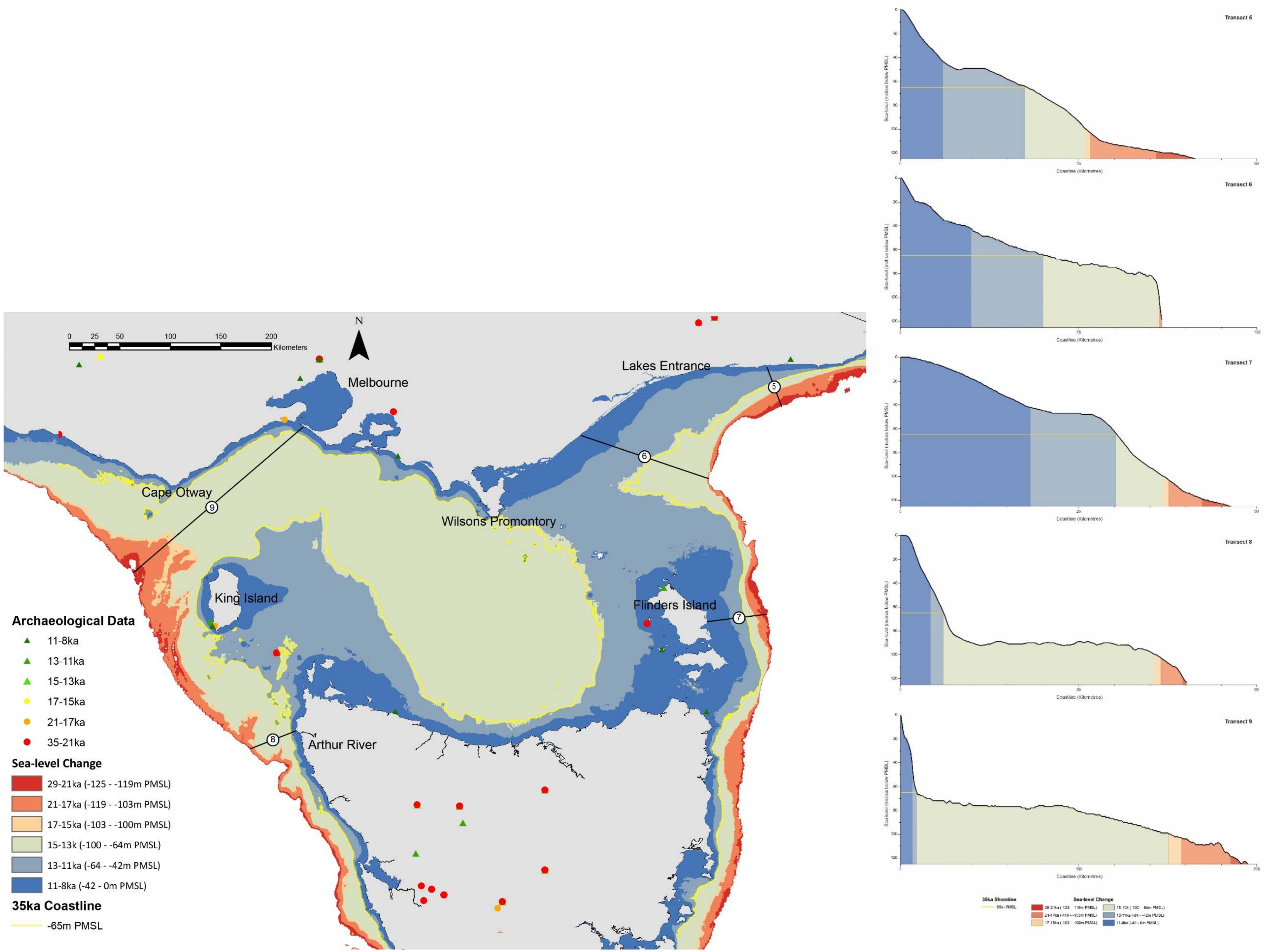

Figure S4: Sea-level and cross section transects 5-9 inclusive, located across Bass Strait.

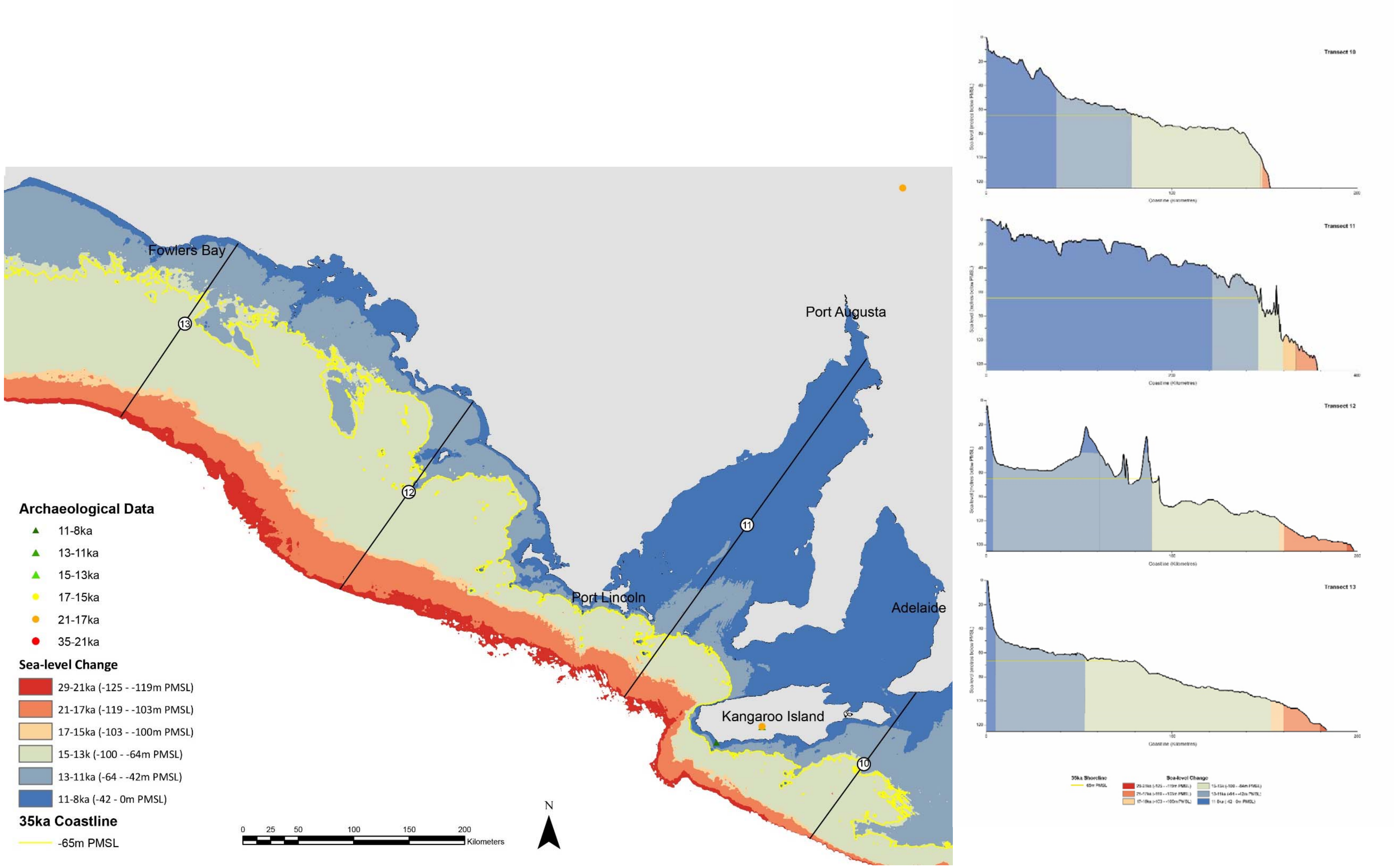

Figure S5: Sea-level and cross section transects 10-13 inclusive, located along the Australian Bight.

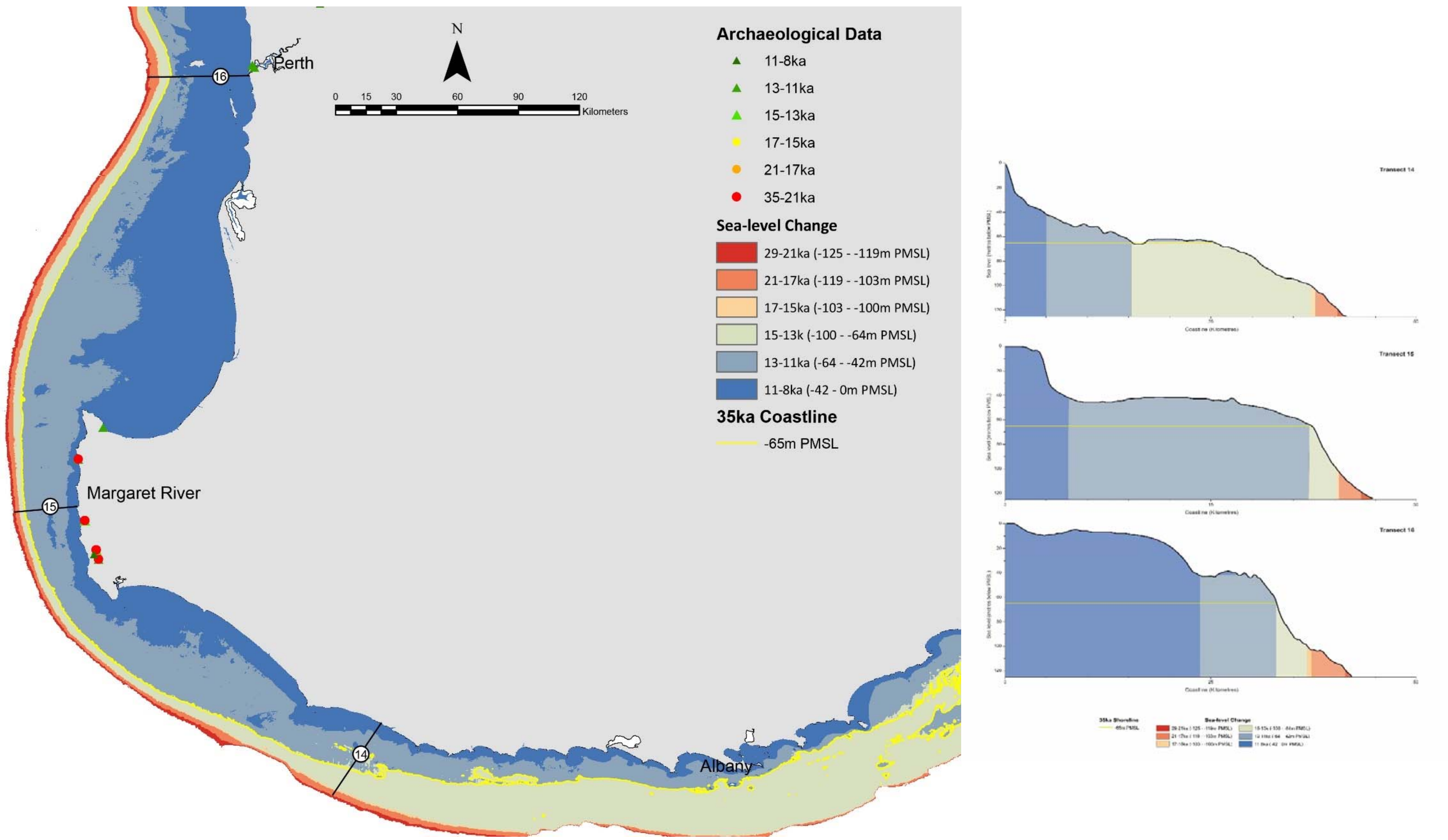

Figure S6: Sea-level and cross section transects 14-16 inclusive, located in southwest western Australia.

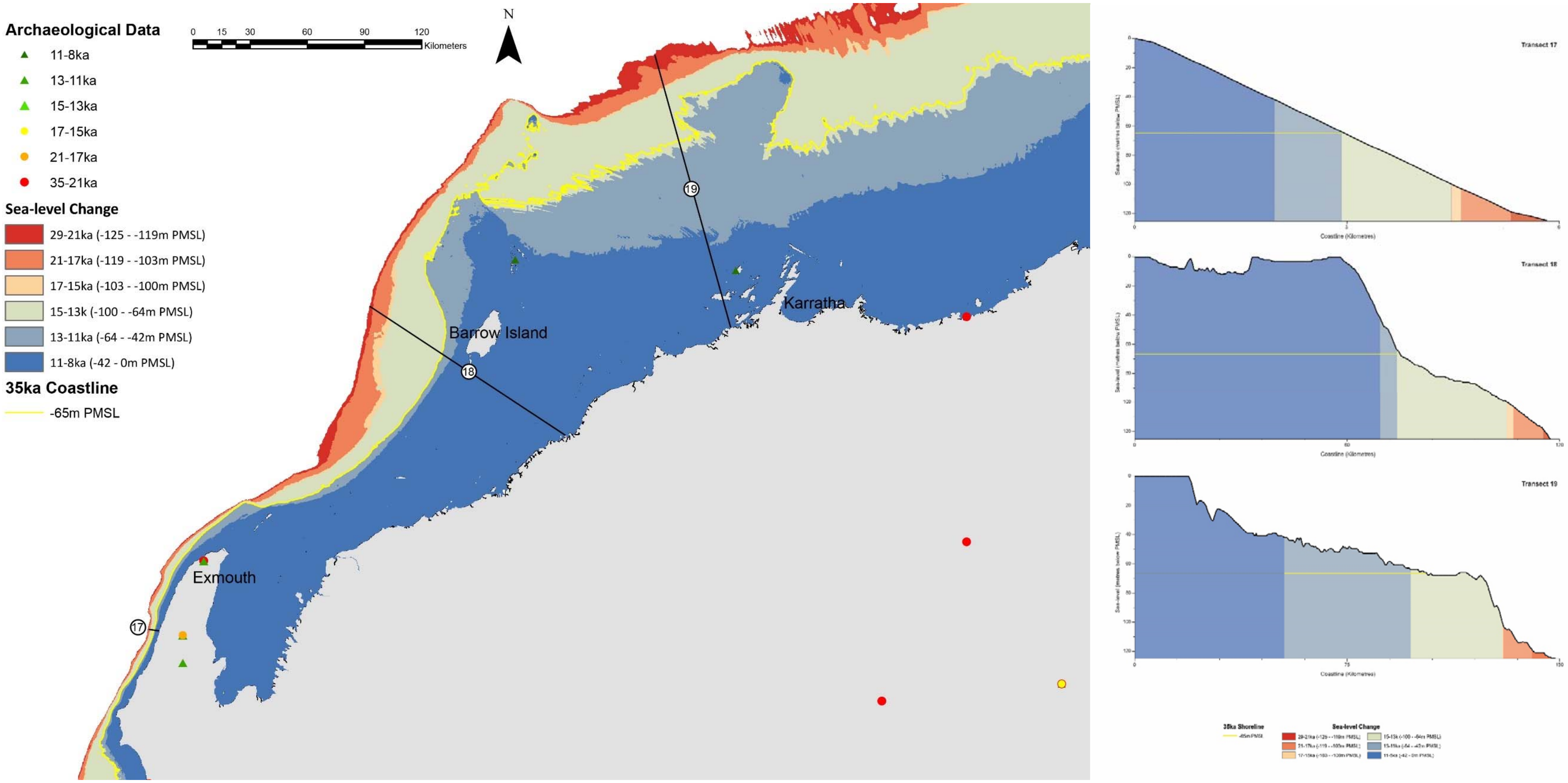

Figure S7: Sea-level transects 17-19 inclusive, located along the Pilbara Coast. Cross sections are presented in Figure S17.

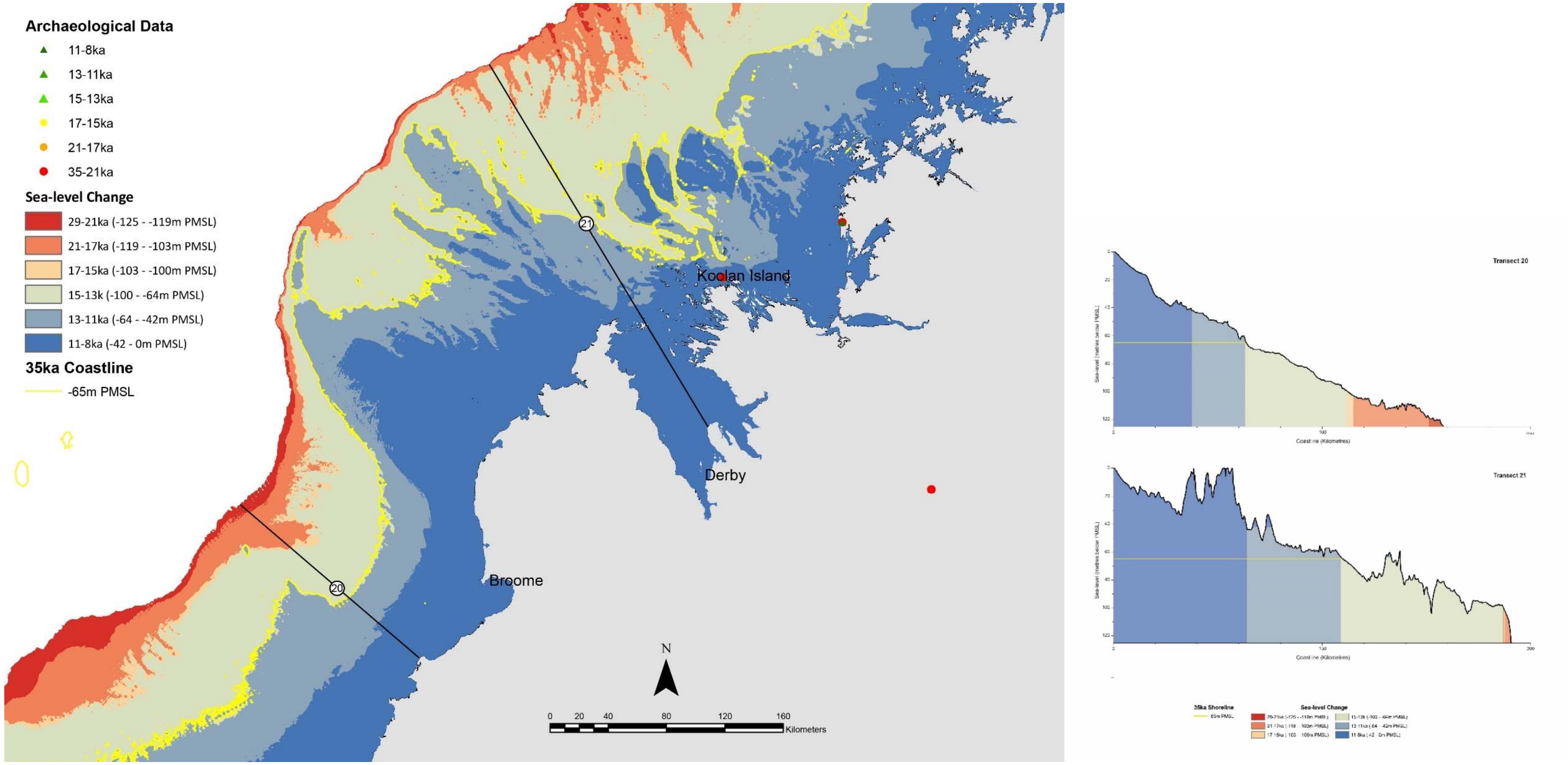

Figure S8: Sea-level and cross section transects 20 and 21, located near Broome and Cape Leveque.

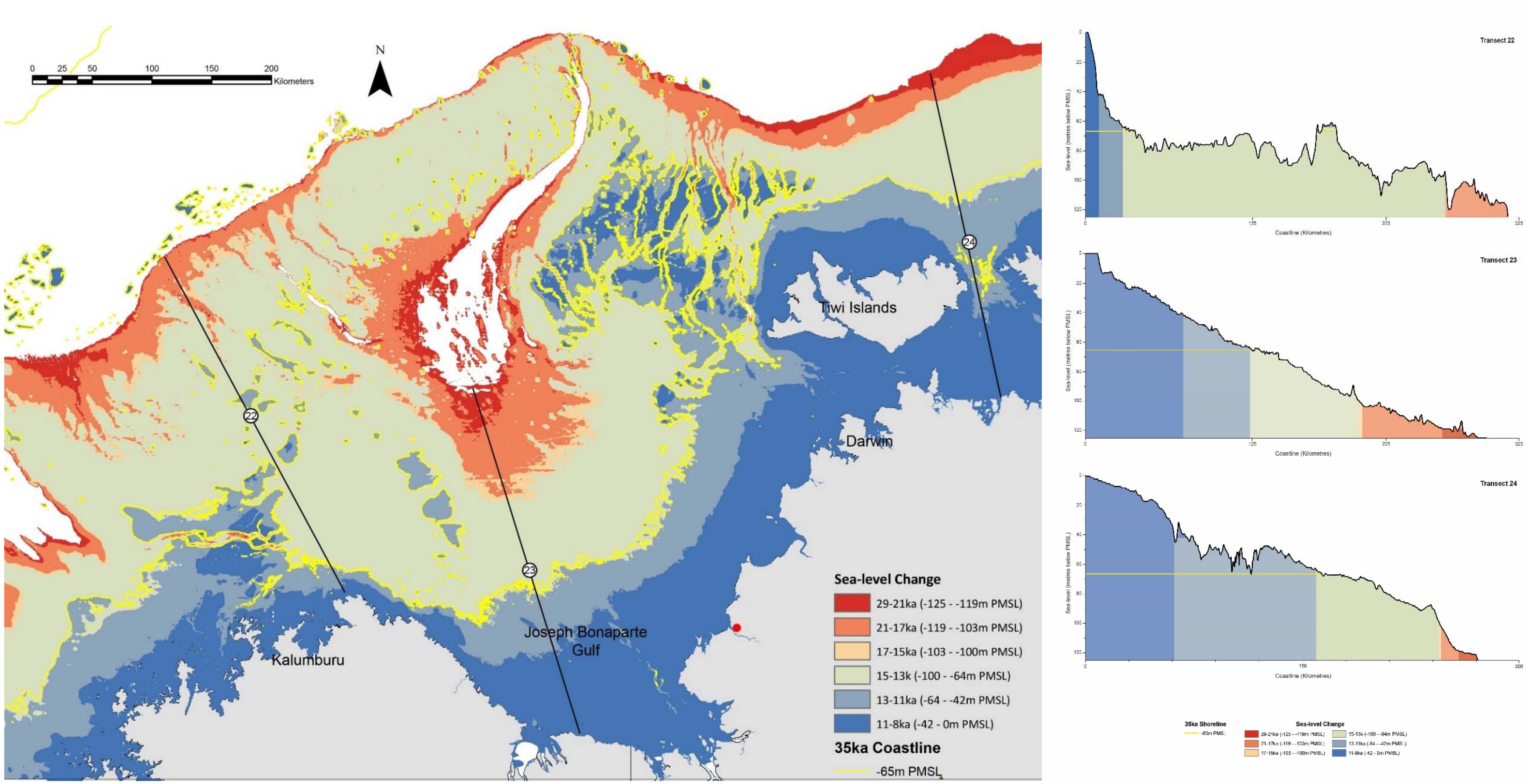

Figure S9: Sea-level and cross section transects 22-24 inclusive, encompassing Joseph Bonaparte Gulf, Tiwi Islands and Darwin.

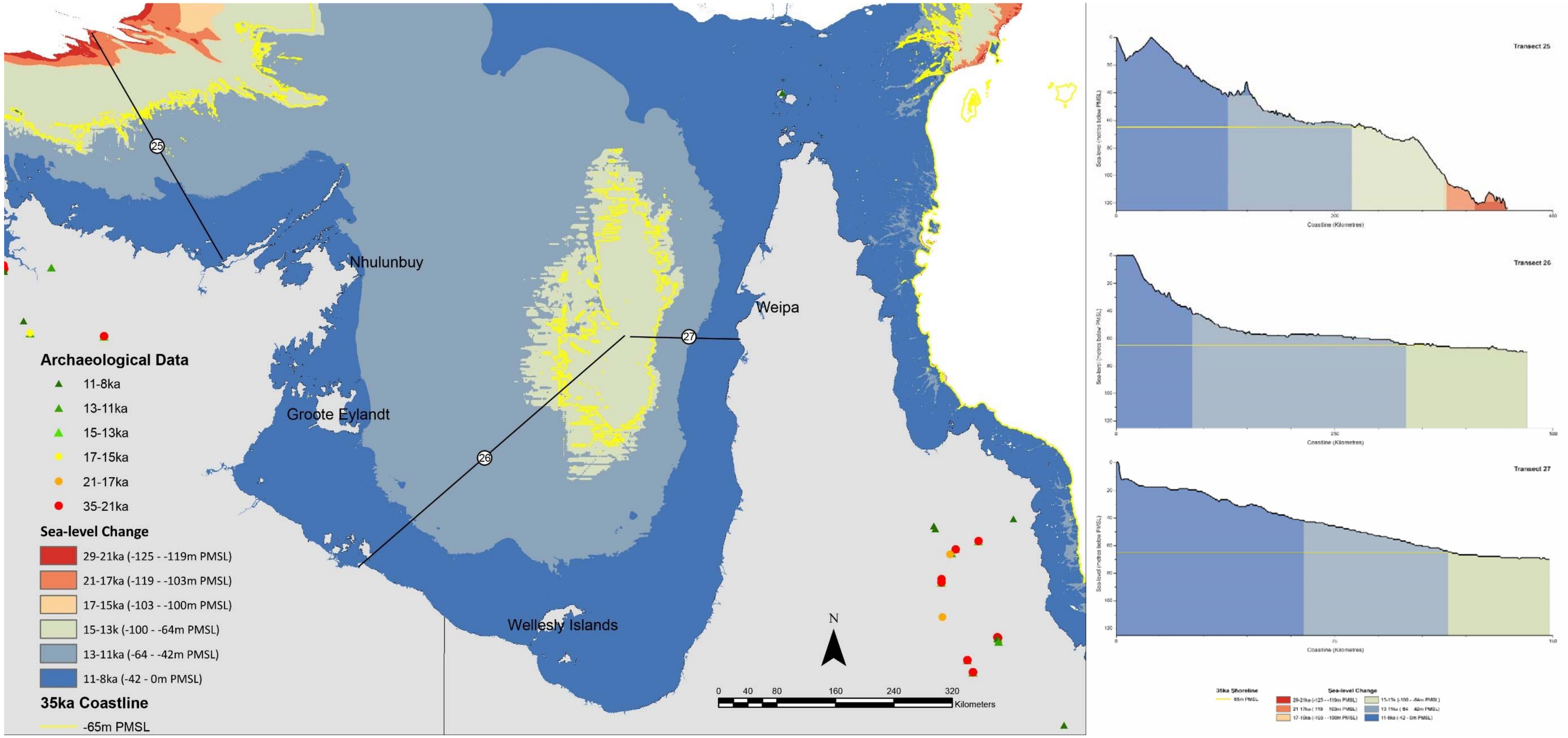

Figure S10: Sea-level and cross section transects 25-27 inclusive, encompassing the Gulf of Carpentaria.

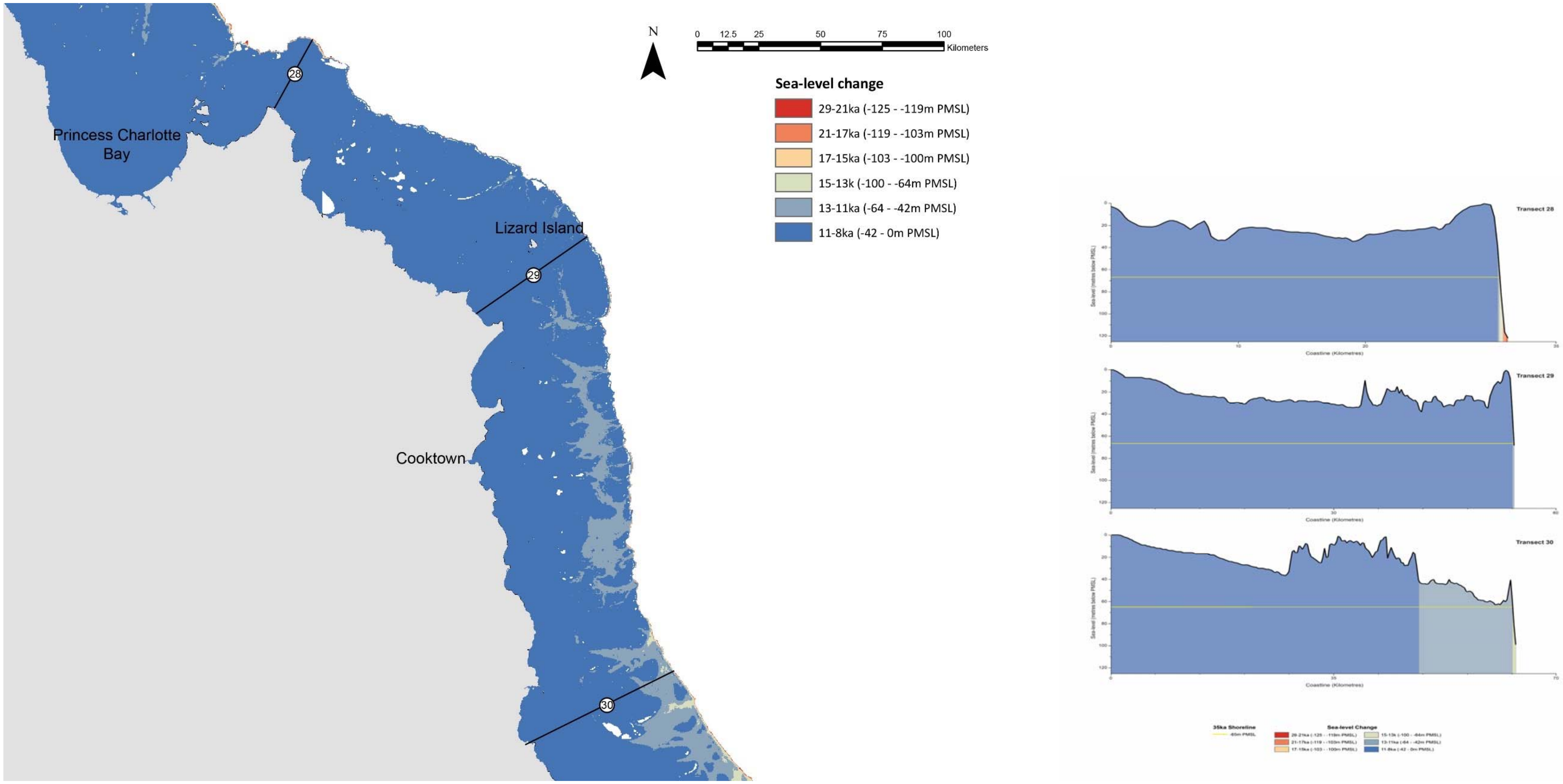

Figure S11: Sea-level and cross section transects 28-30 inclusive, encompassing Princess Charlotte Bay and Cooktown.

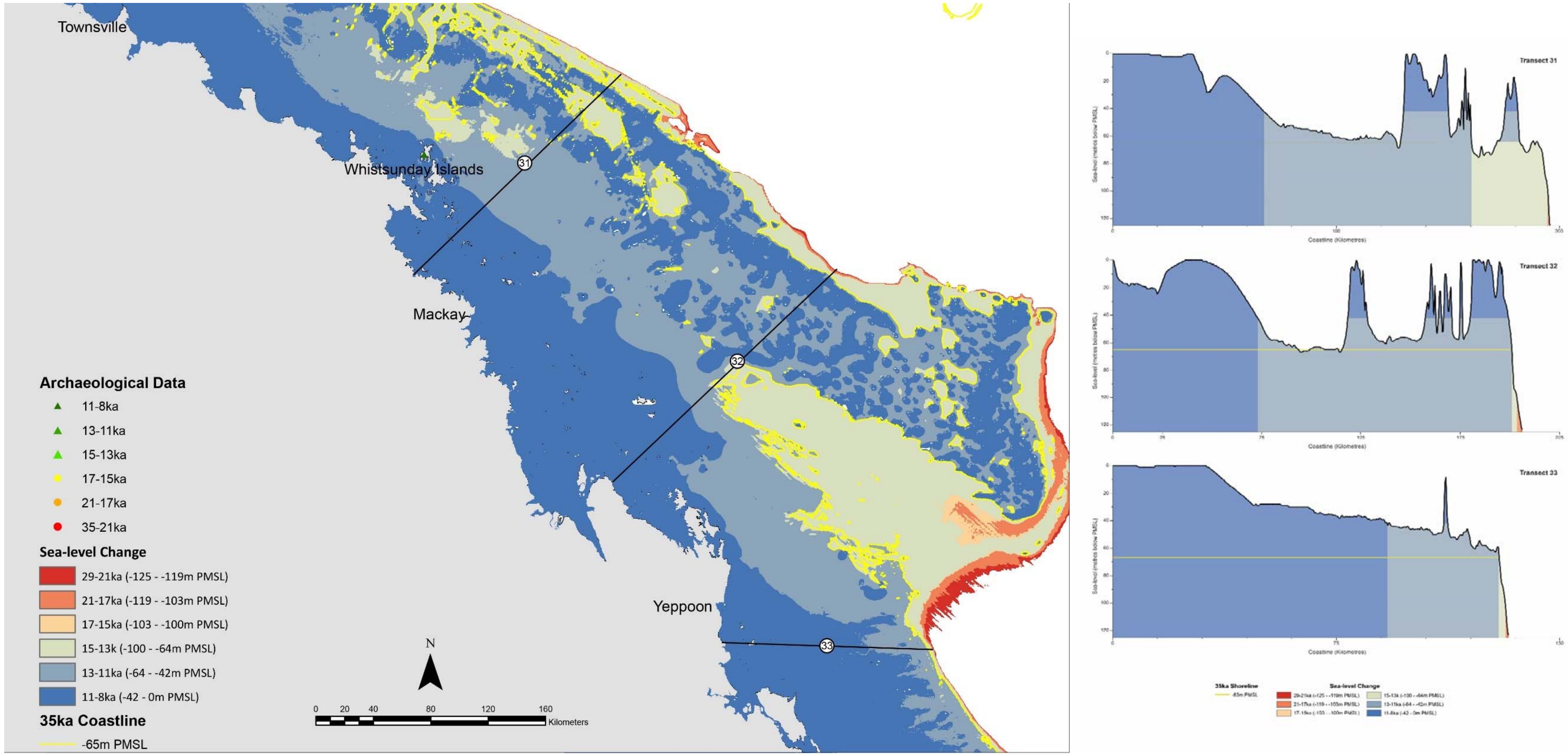

Figure S12: Sea-level transects 31-33 inclusive, encompassing the Whitsunday Islands and Yeppoon. Cross sections are presented in Figure S20.

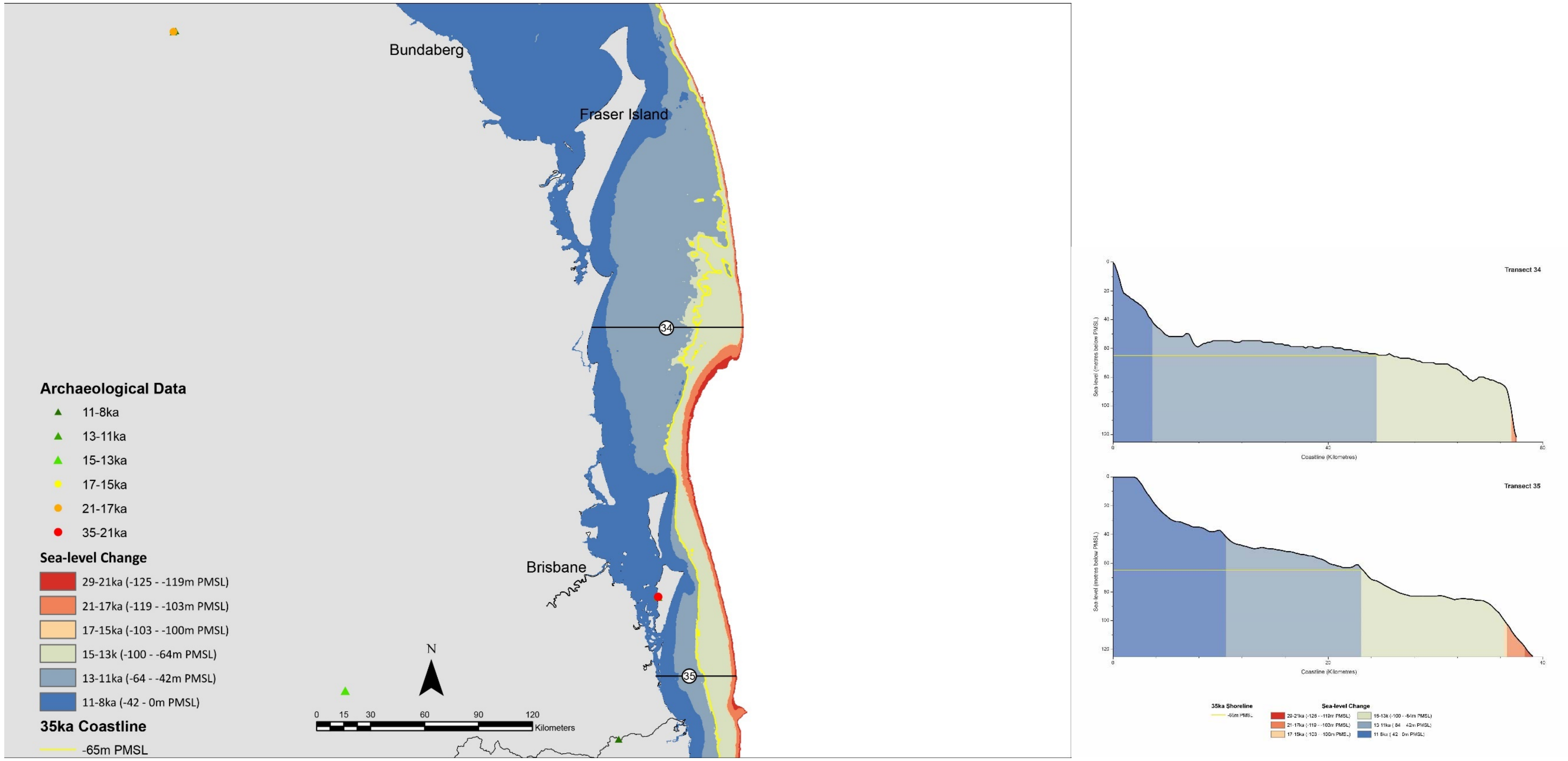

Figure S13: Sea-level and cross section transects 34 and 35, including Fraser Island and Brisbane.

Table S3: Shore-line movements (metres) between 35-8 ka, calculated from 35 transects around the continent. Details of the shore-line changes within each transect are presented below by time period. Transects are shown in Figure S3 – S20. Average, maximum, and minimum values are presented, along with changes per generation (25-years) and annually.

Transect	Time interval (ka)							Total (35-8 ka)	Total (29-8 ka)	Total (15-8 ka)
	35-29	29-21	21-17	17-15	15-13	13-11	11-8			
1	26,183	-1,612	-11,489	-2,077	-11,966	-3,746	-2,641	-7,348	-33,531	-18,353
2	15,256	-6,570	-2,586	-809	-4,904	-2,659	-7,295	-9,567	-24,823	-14,858
3	12,240	-5,989	-3,710	-325	-4,076	-2,667	-5,895	-10,422	-22,662	-12,638
4	11,253	-2,673	-2,845	-174	-6,272	-4,353	-8,072	-13,136	-24,389	-18,697
5	23,877	-5,184	-8,924	-789	-9,130	-12,629	-5,693	-18,472	-42,349	-27,452
6	50,455	-212	-659	-267	-52,018	-35,536	-26,212	-64,449	-114,904	-113,766
7	14,457	-2,167	-5,149	-2,145	-6,932	-12,163	-17,224	-31,323	-45,780	-36,319
8	33,608	-502	-2,146	-1,380	-28,548	-1,985	-4,701	-5,654	-39,262	-35,234
9	185,704	-11,268	-31,714	-7,261	-144,258	-2,595	-5,545	-16,937	-202,641	-152,398
10	70,957	-593	-1,753	-796	-71,994	-36,901	-36,642	-77,722	-148,679	-145,537
11	65,125	-1,712	-23,131	-4,597	-42,282	-61,172	-182,957	-250,726	-315,851	-286,411
12	103,918	-4,566	-34,908	-2,775	-90,934	-62,442	-2,712	-94,419	-198,337	-156,088
13	119,231	-7,266	-19,657	-7,912	-95,261	-48,048	-4,602	-63,515	-182,746	-147,911
14	16,168	-1,004	-2,481	-662	-11,949	-17,570	-8,212	-25,710	-41,878	-37,731
15	5,488	-1,245	-1,660	-189	-1,924	-17,616	-4,792	-21,938	-27,426	-24,332
16	9,414	-1,300	-3,248	-786	-4,467	-2,653	-29,656	-32,696	-42,110	-36,776
17	3,104	-289	-599	-211	-1,212	-1,010	-1,842	-2,059	-5,163	-4,064
18	39,043	-1,983	-9,549	-2,475	-32,148	-4,520	-63,092	-74,724	-113,767	-99,760
19	46,704	-8,274	-8,479	-627	-34,463	-51,549	-43,475	-100,163	-146,867	-129,487
20	94,465	-8,903	-26,966	-3,158	-56,997	-35,793	-31,721	-69,073	-163,538	-124,511
21	123,090	-391	-4,301	-1,413	-117,302	-52,526	-108,855	-161,698	-284,788	-278,683
22	290,833	-1,008	-16,456	-5,922	-260,566	-19,813	-7,767	-20,699	-311,532	-288,146
23	174,792	-15,308	-58,801	-17,552	-83,717	-49,835	-70,854	-121,275	-296,067	-204,406
24	111,537	-13,765	-12,286	-1,615	-82,964	-102,060	-64,014	-165,167	-276,704	-249,038
25	136,179	-6,605	-51,706	-4,692	-73,550	-151,326	-79,798	-231,498	-367,677	-304,674
26	87,381	-	-	-	-136,287	-241,271	-83,060	-373,237	-460,618	-460,618
27	41,840	-	-	-	-44,709	-50,945	-57,196	-111,010	-152,850	-152,850
28	540	-	-359	-	-420	-	-31,146	-31,385	-31,925	-31,566
29	303	-	-	-	-316	-	-53,272	-53,285	-53,588	-53,588
30	323	-	-	-	-393	-14,606	-47,936	-62,612	-62,935	-62,935
31	11,289	-300	-652	-	-30,730	-73,359	-88,100	-181,852	-193,141	-192,189
32	22,983	-746	-1,838	-237	-27,769	-59,398	-118,371	-185,376	-208,359	-205,538

Transect	Time interval (ka)							Total (35-8 ka)	Total (29-8 ka)	Total (15-8 ka)
	35-29	29-21	21-17	17-15	15-13	13-11	11-8			
33	3,705	-521	-695	-3,300	-	-36,523	-91,391	-128,725	-132,430	-127,914
34	22,821	-242	-778	-259	-24,246	-43,154	-7,921	-53,779	-76,600	-75,321
35	17,937	-691	-1,507	-490	-14,674	-12,344	-9,665	-21,434	-39,371	-36,683
Minimum (m)	303	-212	-359	-174	-316	-1,010	-1,842	-2,059	-5,163	-4,064
Maximum (m)	290,833	-15,308	-58,801	-17,552	-260,566	-241,271	-182,957	-373,237	-460,618	-460,618
Average (m)	56,920	-3,763	-11,324	-2,583	-47,335	-40,144	-40,352	-82,660	-139,580	-124,185
Average movement per generation (m)	203.29	-11.76	-70.77	-32.28	-591.68	-501.81	-336.27	-76.54	-166.17	-443.52
Average movement per year (m)	8.13	-0.47	-2.83	-1.29	-23.67	-20.07	-13.45	-3.06	-6.65	-17.74

Past Hunter-Gatherer Demography

Radiocarbon Data as a Proxy for Human Activity

Note that the use of radiocarbon data as a proxy for human activity and associated issues related to time-series analysis have been exhaustively explored in Williams (2012) and (2013), and Williams and Ulm (2016). Extracts of these publications have been included below, but we direct readers with concerns in relation to the application of radiocarbon data as such a proxy to these publications for further details.

One of the key aims of Williams (2012) was to determine how reliable the radiocarbon dataset was in providing a proxy for prehistoric human activity. It is a fundamental assumption that radiocarbon dates used in these analyses derive from occupation events.

This assumption is intrinsic to selection of archaeological samples for dating. A direct association is clearly evident for (a) dated hearths and fireplaces, burials, and shell middens but is less secure for (b) detrital charcoal from occupation deposits (which provide the majority of dates in archaeological datasets). The latter are generally assumed to be charcoal from human activity (e.g. from dispersed fireplaces). This is supported by the correlation between charcoal concentration and the density of other occupation debris (such as lithics and faunal bone) observed in most sites (e.g. Smith (2006): Figure 19). Further support is provided by comparison and statistical correlation of summed probability plots for dated features (group (a) above) and detrital charcoal (Figure S14) showing that both record similar trends in Australian data. Pearson correlation coefficients of these data showed a significant correlation between trends shown in radiocarbon plots for occupation features and detrital charcoal over the last

20,000 years (Table S4 and Figure S14). The correlation was weaker prior to 20,000 years, reflecting the smaller number of dates in these samples, rather than necessarily a de-coupling of the relationship.

Table S4: Pearson correlation coefficient and significance for various time intervals, comparing radiocarbon data for occupation features and detrital charcoal.

Period (cal. yrs BP)	Pearson correlation (*r*)	*P*-value
0 – 9,999	0.686	0.000
10,000 – 19,999	0.341	0.000
20,000 – 29,999	-0.290	0.069
30,000 – 40,000	0.349	0.025
Overall	0.341	0.000

Williams (2013) re-explored this issue with the continental wide radiocarbon dataset (n=4,575). The aim was again to identify whether the entire dataset or a subset from (a) above would provide the most reliable results for reconstructing prehistoric population. It was also undertaken using several new procedures proposed by Peros et al. (2010) to address similar issues in their dataset. These investigations consisted of three different approaches:

1. Comparison of the entire dataset with a subset of those dates containing laboratory errors <100 years. Peros et al. proposed this approach to determine whether unusually large errors in some data significantly impacted the eventual probability distributions/histograms produced.
2. Comparison of the entire dataset with a subset of dates that could be directly correlated to human activity (e.g. burials, hearths, midden material, etc). This comparison was similar to those undertaken in Williams (2012) described above and was undertaken to address the concerns over the large number of detrital charcoal dates in archaeological sequences.
3. Comparison of the entire dataset with a subset of 'occupation events'. These events were coined by Peros et al. (2010) to avoid the common issue of archaeological site duplication, and remove artificial peaks from the data due to multiple dates of the same archaeological feature, etc. The method involved the counting of each site only once per 200-year data bin, regardless of the number of times it appeared, and thereby remove multiple dates from the same stratigraphic unit or feature.

Comparison of the overall dataset with filtered subsets (1-3 above) show good correlation (Figure S15). Each subset contains at least 50% of the overall data and demonstrates similar trends. The occupation event subset contains the highest number of dates within a single subset (n=3,711 or 81%) and indicates that archaeological sample duplication is not a significant issue within the data. A Lin's Concordance Coefficient test between the overall dataset and each subset indicates r values between 0.77 and 0.97, with reduced r values stemming from lack of early data (>20 ka) in some subsets, rather than necessarily de-coupling of the relationship. This correlation suggests that removing dates with >100-year laboratory errors, or from detrital charcoal has little effect on the overall shape of the curve. For this reason, we used the entire dataset in subsequent analysis.

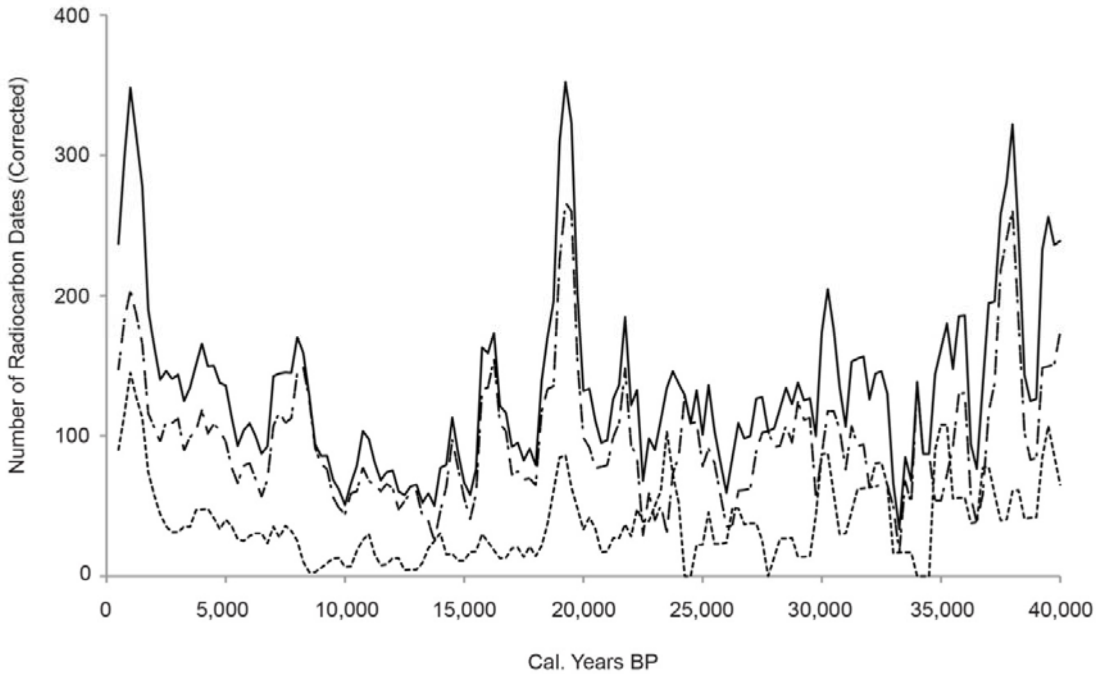

Figure S14: Number of radiocarbon dates for the Williams (2012) dataset (solid line), detrital charcoal subset (dot and dashed line) and a subset of known occupation features such as hearths, midden, burials, etc (dashed line), corrected in accordance with taphonomic correction outlined in Williams (2012). Data presented as 3-point moving average (equivalent to 750 years). A statistical analysis of the overall dataset and the two subsets reveal close correlation over the last 20,000 years. This can be seen most clearly in the Holocene where all data shows similar trends, albeit at different magnitudes.

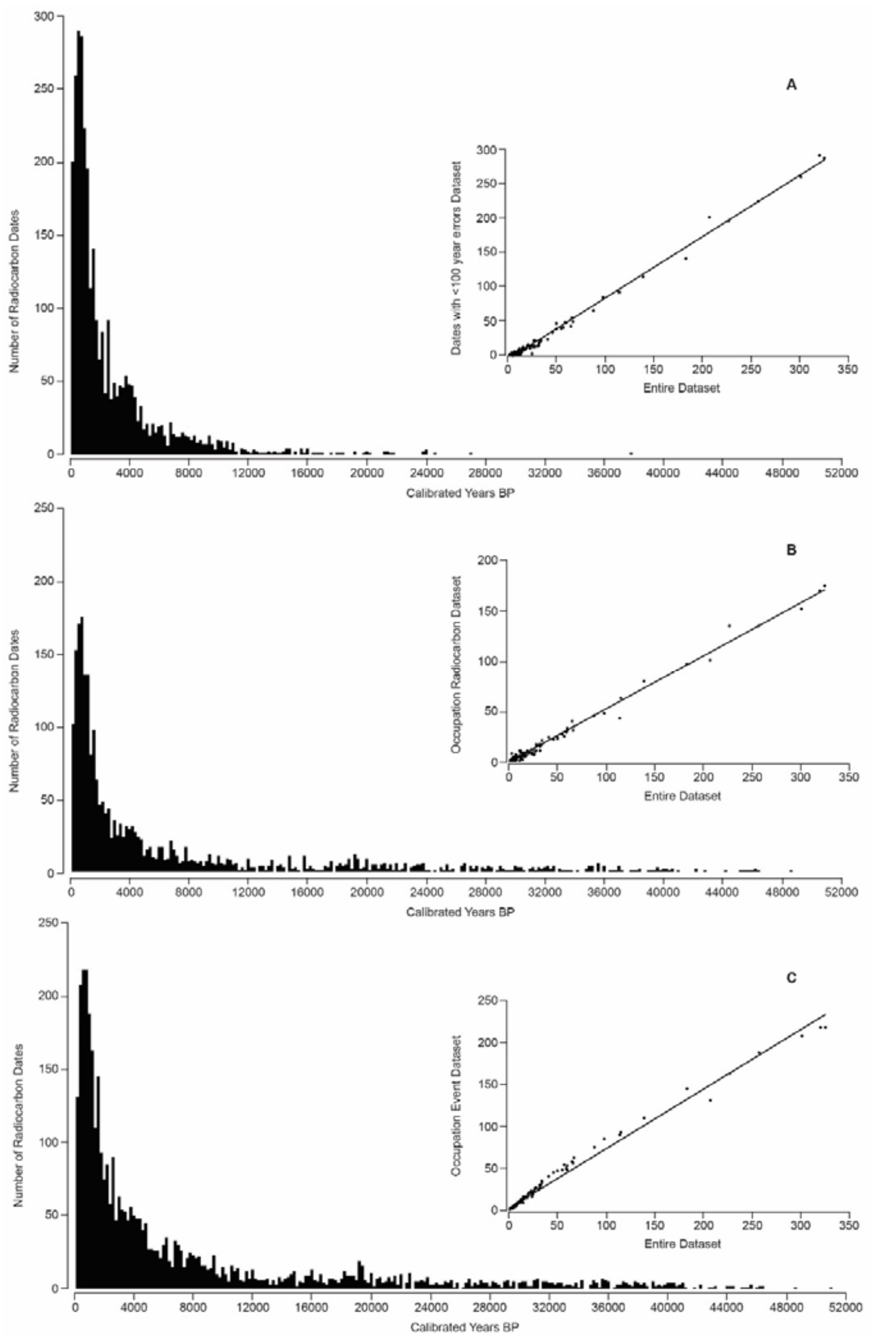

Figure S15. Plots showing only those radiocarbon data that: A) demonstrate errors less than 100 years; B) demonstrate a direct link to occupation activities (e.g. hearths, burials, middens, etc); and C) could be identified as 'occupation events' after Peros et al. (2010). The insets show linear regression between each subset and the overall uncorrected dataset. A Lin's concordance coefficient analysis of these data indicate good correlation (r values as follows: A = 0.977; B = 0.770; C = 0.925) and demonstrate that the overall dataset provides a reliable curve for prehistoric activity.

Radiocarbon Calibration

All radiocarbon data were calibrated using using Oxcal (version 4.1) (Bronk Ramsey, 2009). Terrestrial dates were calibrated using INTCAL13 and marine dates using MARINE13 (Reimer et al., 2013) with ΔR values after (Ulm, 2002, 2006). Oxcal was used to both obtain a median value for each radiocarbon date (95.4% confidence) and to create sum probabilities. To remove some of the calibration anomalies and allow subsequent analysis, each calibrated date was then 'data binned' into 200-year intervals based on its median value. We acknowledge that when calibrating a radiocarbon date, the age may occur anywhere within the minimum and maximum values provided by the calibration program (rather than the median value). However, on average, calibrated ages in the dataset had less than a 452-year range, and would have remained within the same broad time slices applied in the dataset, regardless of which part of the calibrated age range was selected

Taphonomic correction

Where taphonomic correction is referenced in relation to radiocarbon data, it is based on procedures in Williams (2012, 2013). This procedure involves correction of the actual number of dates per 200-yr bin using a decay curve created from a volcanic radiocarbon dataset. The correction equation is:

$$n_c = n_a/(2.107 \times 10^7(t + 2754)^{-1.526}) \qquad \text{(S1)}$$

where n_c = taphonomically corrected number of radiocarbon dates for the dataset of interest, n_a is the actual number of radiocarbon dates present at a specific time (t) in the dataset of interest. After Williams (2013), we combined 'corrected' open site data and 'uncorrected' data from rockshelters to develop the overall curves.

Development of annual average growth rates and palaeo-populations

Peros et al. (2010) used radiocarbon data to develop quantitative palaeo-Indian population estimates for North America. Using more than 25,000 radiocarbon dates spread across the continent, Peros et al. (2010) developed a method of converting numbers of radiocarbon dates into an average annual change in population through time (GR_{Ann}). They then applied this equation to a range of founding populations to estimate the population of palaeo-Indians through time. Here the same approach was used to develop similar prehistoric population estimates in Australia.

The method developed by Peros et al., first included the calibration of all radiocarbon data. Using the median value, each date was then divided into 200-year data bins of 'number of dates'. (Data-binning is a form of quantization – mapping a large set of input values into a smaller set and reducing minor observational error). A smoothing spline was then run through the data bins, with subsequent analysis using interpolated values from this spline. The reason for the introduction of the spline and use of interpolated values was two-fold: 1) it removed extreme values and outliers from the data-bins; and 2) most importantly it removed zero values from the data, which are problematic when applying Eq. (S2). In relation to (1), this was controlled by the degrees of freedom (df) used to develop the spline; a lower df reducing the extreme values in the data. Peros et al. adopted a df value- of 25 for their analysis, whereas for this analysis a range of df values (15-200) were explored and considered: both 25 and 50 provided a good balance between data variability and coherent results. Using the values interpolated by the spline, Peros et al. applied an equation to determine annual percentage growth rate (GR_{Ann}) as follows:

$$GR_{Ann} = 0.5((d2 - d1)/d1) \qquad \text{(S2)}$$

where in a given pair of consecutive 200-yr data bins, d2 is the number of radiocarbon dates in the younger bin, and d1 is the number of dates in the older bin. Each GR_{Ann} value was multiplied by 0.5 to convert to a percentage (i.e. multiply the value by 100) and to produce an annual rate from the 200-year bins (i.e. divide each 200-year bin by 200 to obtain an annual value). In its simplest form Eq. (S2) simply shows the change between each data bin (i.e. number of radiocarbon data per 200 year period divided into annual periods); Peros et al. assumed that the number of radiocarbon dates directly correlated with population, and therefore the changes identified through this equation reflected differences in population growth or decline. Here, we also consider the change in data to reflect a population signal.

While Peros et al. use the GR_{Ann} to re-create quantitative palaeo-Indian populations, they do not elaborate on the methods used to convert the GR_{Ann} into actual population values. Population estimated used in this paper were taken from Williams (2013) who adopted a simple compound interest equation used commonly in the fields of banking and economics to the GR_{Ann} values:

$$P = f(1+GR_{Ann})^t \qquad \text{(S3)}$$

where P is final population, f is initially the founding population followed by the P value from each preceding 200-year data bin, the GR_{Ann} is the relevant Eq. (S2) associated with each 200-year bin, and t is number of years. The equation was then applied to each 200-year data bin and associated GR_{Ann} value through time to create population change from 50 ka to Contact. So once an initial founding population (see below) was entered into the equation at 50-49.8 ka (the first 200-year data bin in this analysis) and the relevant GR_{Ann} applied, the result of this analysis is then placed into the same equation as f for the 49.8-49.6 ka data-bin (the second 200-year data bin in this analysis) and the relevant GR_{Ann} value applied, and so on until 0ka is reached. Using a hypothetical example: Introducing a founding population of 100 at 50-49.8 ka data bin and applying a GR_{Ann} of 5% would equate to a final population value of 105 [P=100(1+0.05)200] for this data bin. (Note the GR_{Ann} is presented here as a decimal.) Continuing the example, applying population of 105 to the next data bin (49.8-49.6 ka) with a GR_{Ann} of -10% would result in a final population of 94.5 [P=105(1+-0.10)200]. This approach is applied to each data bin until 0 ka is reached to produce the final population figures outlined in Williams (2013).

Based on a range of factors, Williams (2013) considered colonisation of Australia to occur between 46-50 ka, and developed estimates using this starting point. For founding populations, early researchers considered a small family group or band (<50) was considered likely, whereas recent DNA analysis suggests numbers in the hundreds and probably low thousands were required. Williams (2013) therefore used a range of founding populations (50, 500, 1000, 2000, 3000, 5000) to apply Eq. (S3). Following, a detailed review of demographic literature, Williams (2013) considered that values of between 300,000 to 1 million at European Contact were the most likely, and therefore the founding populations applied to Eq. (S3) were used to reproduce values that fell within this range at 0ka. He found that values in excess of 5,000 people at 50 and 46 ka reproduced Contact populations well in excess (>2 million) of recorded values, and this therefore provided a maximum founding population. Conversely, a founding population of 50 produced very low numbers at time of Contact; and this value therefore formed the lowest founding population tested. The remaining values provided a range between 50 and 5,000 with which to best reproduce Contact populations in accordance with the observed range above (Figure S16). Ultimately, Williams (2013) concluded that founding populations of between 2000-3000 were most likely. A summary of population estimates at key time interval based on these founding populations is presented in Table S5.

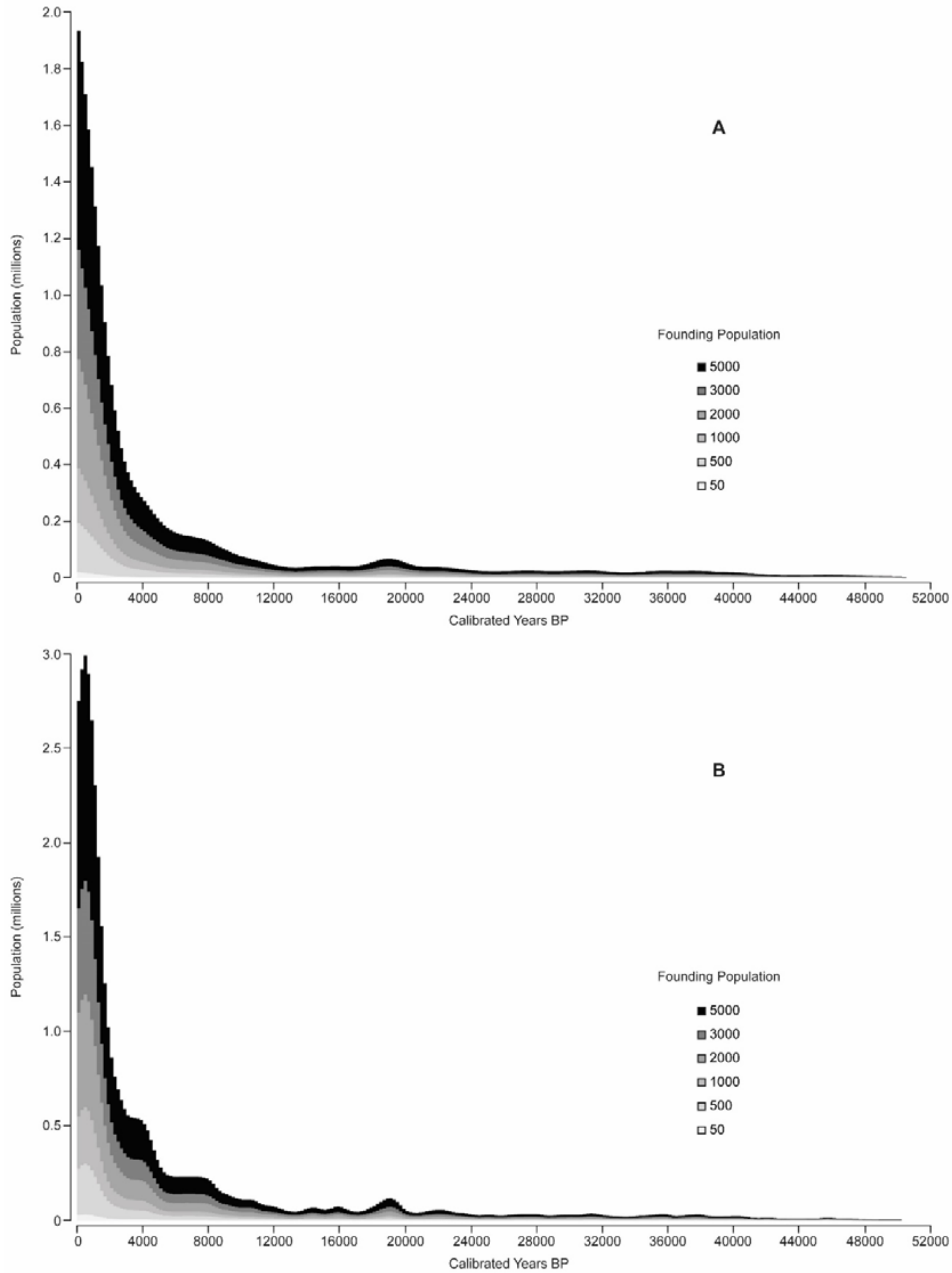

Figure S16. A plot of population estimates from 50 – 0 ka using uncorrected radiocarbon data reproduced from Williams (2013). Each graph was developed by implementing founding populations at 50 ka and applying Eq. (S3). A) Population estimates based on GR_{Ann} values developed using a spline with a *df* = 25; and B) as A but using a spline with *df* = 50.

Table S5. Selected time slices of population estimates from Williams (2013). These values were based on the application of equation (S3) to GR_{Ann} values and a smoothing spline with *df* = 25 (values in brackets used a smoothing spline with *df* = 50). (Founding populations of 1000, 2000, and 3000, and colonization dates of 50 and 46 ka are shown.)

Age (ka)	Population estimates after Eq. (S3) applied from 50 ka			Population estimates after Eq. (S3) applied from 46 ka		
	Founding Population – 1,000	Founding Population – 2,000	Founding Population – 3,000	Founding Population – 1,000	Founding Population – 2,000	Founding Population – 3,000
30	4,784 (5,793)	9,568 (11,586)	14,352 (17,379)	2,523 (2,959)	5,047 (5,919)	7,571 (8,878)
16	8,235 (13,800)	16,471 (27,601)	24,707 (41,402)	4,344 (7,050)	8,689 (14,101)	13,304 (21,152)
8	25,389 (42,086)	50,778 (84,173)	76,168 (126,259)	13,393 (21,501)	26,787 (43,003)	40,180 (64,504)
4	53,915 (102,213)	107,831 (204,427)	161,746 (306,641)	28,442 (52,220)	56,884 (104,440)	85,326 (156,661)
0.5	341,604 (598,211)	683,209 (1,196,423)	1,024,814 (1,794, 634)	180,206 (305,623)	360,412 (611,246)	540,619 (916,869)

Development of Hunter-Gatherer 'Territories'

The investigation of the amount of land used by hunter-gatherers in the past is based on the works in Williams et al. (2013) and (2015). The analysis in these publications used calibrated radiocarbon data and cluster analysis to identify the spatial area of land that was used by past populations at any given time period. The procedure in these publications is reproduced below.

Spatial analysis of the median calibrated radiocarbon values was undertaken in ArcGIS, R and Geospatial Modelling Environment (GME) software using a three-step process after the method outlined by Chilès and Delfiner (2012). These steps are 1) allocating points to over-lapping time slices, 2) K-means cluster analysis, and 3) cluster centroid and point dispersal pattern analysis.

The purpose of using over-lapping time slices was to divide the dataset into discrete time slices for use in K-means analysis, by removing points associated with radiocarbon ages that were considered statistically distinct. Given the low number of data available for the analysis, it was considered that the loss of data through the use of firm slices was unacceptable and over-lapping ones were instead adopted. In addition, trials indicated that using firm time slices would have increased the number of dates with calibration age ranges outside their respective slice, and increased uncertainty in the results. (It is highlighted that the two publications use slightly different time-slice intervals, with more abundant data in the Holocene allowing a finer resolution and 500-year firm time-slices adopted).

Over-lapping time slices were created by using Moran's Local I test (Anselin, 1995) to remove any spatial outliers within a 2,000-year time slice, commencing with all calibrated radiocarbon dates between 25 – 23 ka BP. Subsequently, the mean and standard deviation of calibrated dates at the same location was calculated and any points with values greater than mean ± 1 SD were removed and re-evaluated within the next chronologically younger time slice. Following this assignment of data to individual time slices, all points were converted into a $10km^2$ grid and then back into points in order to 'average' calibrated data values within local neighbourhoods, and to de-cluster the dataset removing bias from the subsequent K-means analysis. This stage was used to ensure that areas where archaeological research has been extensive, multiple LGM dates have been obtained from the same site, and/or Pleistocene landscapes are readily apparent (e.g. Murray Darling Depression) did not overwhelm the analysis and mask any real trends. $10km^2$ was considered the optimum size, with a range of larger grid sizes continuing to retain bias in subsequent stages of the analysis. No point was used more than once in the entire analysis.

After data were allocated to the time slices, a partitioning clustering technique, K-means, was implemented (Hartigan, 1975, 1977). K-means clustering is a statistical method for grouping data. It aims to partition *n* observations into *k* clusters in which each observation belongs to the cluster with the nearest mean (in our case the latitude and longitude position of the point). The output of the analysis is a centroid representing the centre point (mean latitude and longitude) of the observations included in the cluster, along with a rectangle that represents the minimum bounding extent of all observations included in that cluster. K-means is an iterative process in which points are assigned to a predetermined number of clusters (*k*) beginning with an initial 'seeding point' selected by automated stochastic process (Connolly and Lake, 2006). Points are subsequently allocated to the cluster they are nearest to and as new points are added, the centre of the cluster is re-defined and the point-cluster relationship re-evaluated to a maximum number of iterations (n=100). The results are evaluated by studying the squared Euclidean distances between each point and their respective cluster centroid. Williams et al. (2013) and (2015) used the 'elbow' method to determine the optimum number of clusters to explain the data. In statistical terms the elbow represents the point where percentage variance against the number of clusters reaches a threshold where adding another cluster does not reduce overall variance, and therefore ceases to give a much better model of the data (see Chiang and Mirkin 2007 for an evaluation of techniques). Relative to other clustering techniques, K-means strength is faster and produces more discrete clusters. However, it is a stochastic process, so it may not yield the same results on each model run (the stochasticity arises as the initial seeding point is generated randomly in dimensionless space). This is addressed by re-running the model with the same parameters and performing diagnostic checks on any systematic inconsistencies. Ultimately the analyst must exercise judgement in relation to the number of clusters.

Using the K-means results, the final stage of the analysis was to evaluate changes to the cluster centroid and point dispersal pattern. The point dispersal pattern is visualised by creating minimum bounding rectangles (MBR) - the rectangle demonstrates which points are assigned to which cluster centroid. From an archaeological perspective, these rectangles theoretically represent the range of human groups associated with each cluster centroid. Additional exploration of convex hull approaches were also undertaken. This approach explores the relationship of a point with the cluster centroid through direct measurement of each point back to the centre producing irregular polygons or bounding boxes. The analysis indicated that the convex hull approaches produced very similar trends to the MBRs.

Location and references within the publication

Figure S17 shows the location of archaeological sites and geographic locations mentioned in the publication. References for the archaeological sites are presented in Table S6.

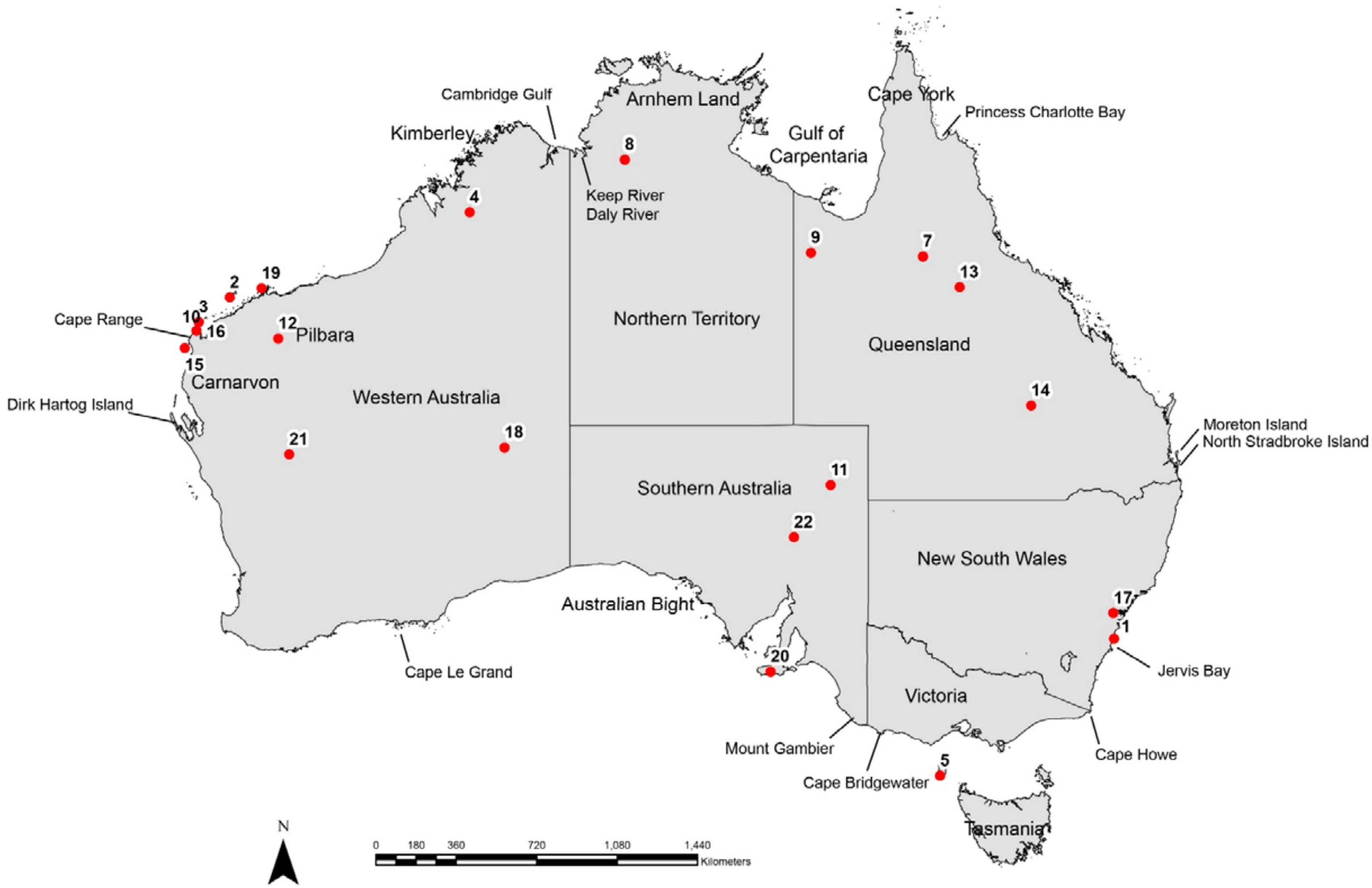

Figure S17. Map of archaeological sites and geographic locations referenced in text. Archaeological sites are presented as unique numbers, which are presented with further details in Table S6.

Table S6. Archaeological site information from Figure S17.

Site ID (Figure S17)	Site	Reference
1	Bass Point	Hughes, P.J., Djohadze, V., 1980, *Radiocarbon Dates From Archaeological Sites on the South Coast of New South Wales and the Use of Depth/Age Curves*. Occasional Papers in Prehistory 1. Canberra, Department of Prehistory, Australian National University.
2	Boodie Cave	Veth, P., Ward, I., Manne, T., Ulm, S., Ditchfield, K., Dortch, J., Hook, F., Petchey, F., Hogg, A., Questiaux, D., Demuro, M., Arnold, L., Spooner, N., Levchenko, V., Skippington, J., Byrne, C., Basgall, M., Zeanah, D., Belton, D., Helmholz, P., Bajkan, S., Bailey, R., Placzek, C., Kendrick, P., 2017. Early human occupation of a maritime desert, Barrow Island, north-west Australia. *Quat. Sci. Rev.* **168**, 19-29.
3	C99 rockshelter	Przywolnik, K., 2002. Patterns of Occupation in Cape Range Peninsula (WA) over the last 36,000 years. Unpublished PhD thesis, Centre for Archaeology, University of Western Australia, Perth.
4	Carpenter's Gap rockshelter 1	O'Connor, S., 1995. Carpenter's Gap Rockshelter 1: 40,000 years of Aboriginal occupation in the Napier Ranges, Kimberley, WA. *Aust. Archaeol.* **40,** *58-59*.
5	Cliff Cave	Sim, R., 1994. Prehistoric human occupation in the King and Furneaux Island regions, Bass Strait, in: Sullivan, M., Brockwell, S., Webb, A., (Eds.), *Archaeology in the North. Proceedings of the 1993 Australian Association Conference*. Northern Australia Research Unit, The Australian National University, Darwin, pp. 358-374
7	Gledswood rockshelter 1	Wallis, L., Keys, B., Moffat, I, Fallon, S., 2009, Gledswood Rockshelter 1: Initial Radiocarbon Dates from a Pleistocene Rockshelter Site in Northwest Queensland. *Aust. Archaeol.* **69,** 71-74.
8	Gordolya rockshelter	Clarkson, C., 2007. *Lithics in the Land of the Lightning Brothers: The Arhaeology of Wardaman Country, Northern Territory*. Terra Australis 25. Canberra, The Australian National University E-Press
9	Gregory River 8	Slack, M.J., Fullagar, R.L.K., Field, J.H., Border, A., 2004. New Pleistocene ages for backed artefact technology in Australia. *Archaeol. in Ocean.* **39(3),** 131-137.
10	Jansz rockshelter	Przywolnik, K., 2002. Patterns of Occupation in Cape Range Peninsula (WA) over the last 36,000 years. Unpublished PhD thesis, Centre for Archaeology, University of Western Australia, Perth.
11	JSN Site	Smith, M.A., Williams, E., Wasson, R.J., 1991, The Archaeology of the JSN Site: Some Implications for the dynamics of Human Occupation in the Strezelecki Desert during the late Pleistocene. *Records of the South Australian Museum*, **25**: 175-192.

Site ID (Figure S17)	Site	Reference
12	Juukan-1 rockshelter	Slack, M., Fillios, M., Fullagar, R., 2009. Aboriginal Settlement during the LGM in Brockman, Pilbara Region, Western Australia. *Archaeol. in Ocean.* **44,** 32-39.
13	Mickey Springs 34	Morwood, M., 1990. The prehistory of Aboriginal landuse on the upper Flinders River, north Queensland highlands. *Queensland Archaeol. Res.* 7, 3-56.
14	Native Well 1	Morwood, M., 1979, Art and Stone: Towards a Prehistory of Central Western Queensland. 2 vols. Unpublished PhD thesis, Department of Archaeology and Anthropology, Faculty of Arts, Australian National University, Canberra.
15	Noala 1 rockshelter	Veth, P., 1995. Aridity and settlement in northwest Australia. *Antiquity* **69,** 733-746.
16	Pilgonaman Creek rockshelter	Morse, K., 1993. Who can see the sea? Prehistoric Aboriginal occupation of the Cape Range Peninsula, in: Humphreys, W.F., (Ed.), *The Biogeography of Cape Range, Western Australia*. Records of the Western Australian Museum 45. Perth, Western Australian Museum, pp. 227-242.
17	PT-12 open site	Williams, A.N., Atkinson, F., Lau, M., Toms, P., 2014. A Glacial cryptic refuge in southeast Australia: Human occupation and mobility from 36,000 years ago in the Sydney Basin, New South Wales. *J. of Quat. Sci.* **29(8),** 735-748.
18	Puntutjarpa rockshelter	Gould, R.A., 1977. *Puntutjarpa Rockshelter and the Australian Desert Culture*. American Museum of Natural History. Anthropological Papers 54.
19	Rosemary Island	McDonald, J., Berry, M., 2016. Murujuga, Northwestern Australia: When Arid Hunter-Gatherers Became Coastal Foragers. *J. of Island and Coastal Archaeol.* DOI: 10.1080/15564894.2015.1125971.
20	Seton Site	Lampert, R.J., 1977. Kangaroo Island and the antiquity of Australians, in: Wright, R.V.S., (Ed.*) Stone Tools as Cultural Markers: Change, Evolution and Complexity*. Canberra, Australian Institute of Aboriginal Studies, pp. 213-218.
21	Walga Rock rockshelter	Bordes, F, Dortch, C., Thibault, C., Raynal, J.P., Bindon, P., 1983. Walga Rock and Billibong Spring: Two archaeological sequences from the Murchison Basin, Western Australia. *Aust. Archaeol.* **17,** 1-26.
22	Warratyi rockshelter	Hamm, G., Mitchell, P., Arnold, L.J., Prideaux, G.J., Questiaux, D., Spooner, N.A., Levchenko, V.A., Foley, E.C., Worthy, T.H., Stephenson, B., Coulthard, V., Coulthard, C., Wilton, S., Johnston, D., 2016. Cultural innovation and megafauna interaction in the early settlement of arid Australia. *Nat.* **539,** 280-283.

References

Anderson, D.G., Bissett, T.G., 2015. The initial colonization of North America: Sea level change, shoreline movement, and great migrations, in: Frachetti, M.D., Spengler III, R.N., (Eds.), *Mobility and Ancient Society in Asia and the Americas*. Zurich, Springer International Publishing, pp.59-88. doi: 10.1007/978-3-319-15138-0_6.

Anselin, L., 1995. Local Indicators of Spatial Association—LISA. *Geographical Analysis.* 27(2), 93-115.

Bronk Ramsey C., 2009. Bayesian analysis of radiocarbon dates. *Radiocarbon.* **51(1),** 337-360.

Chiang MMT, Mirkin B., 2007. Experiments for the number of clusters in K-means, in: Neves, J., Santos, M., Machado, J., (Eds.), *EPIA 2007*. LNAI 4874. pp. 395-405.

Chilès, J-P., Delfiner, P., 2012. *Geostatistics - Modeling Spatial Uncertainty*. 2nd edition. New Jersey, John Wiley & Sons.

Connolly, J., Lake, M., 2006. *Geographical Information Systems in Archaeology*. Cambridge, Cambridge University Press.

Hartigan, J.A., 1975. *Clustering Algorithms*. New York, John Wiley.

Hartigan, J.A., 1977. Distribution problems in clustering, in: Ryzin, J.V., (Ed.), *Classification and Clustering*. New York, Academic Press. pp. 45-71.

Lambeck, K., Yokoyama, Y., Purcell, T., 2002. Into and out of the Last Glacial Maximum: Sea-level change during Oxygen Isotope Stages 3 and 2. *Quat. Sci. Rev.* **21,** 343-360.

Lewis, S.E., Sloss, C.R., Murray-Wallace, C.V., Woodroffe, C.D., Smithers, S.G., 2013 Post-glacial sea-level changes around the Australian margin: A review. Quat. Sci. Rev. **74,** 115-138. doi:10.1016/j.quascirev.2012.09.006

Peros, M.C., Munoz, S.E., Gajewski, K., Viau, A.E., 2010. Prehistoric demography of North America inferred from radiocarbon data. *J. of Archaeol. Sci.* **37,** 656-664.

Reimer, P.J., Bard, E., Bayliss, A., Beck, J.W., Blackwell, P.G., Bronk Ramsey, C., Buck, C.E., Cheng, H., Edwards, R.L., Friedrich, M., Grootes, P.M., Guilderson, T.P., Haflidason, H., Hajdas, I., Hatté, C., Heaton, T.J., Hoffmann, D.L., Hogg, A.G., Hughen, K.A., Kaiser, K.F., Kromer, B., Manning, S.W., Niu, M., Reimer, R.W., Richards, D.A., Scott, E.M., Southon, J.R., Staff, R.A., Turney, C.S.M., van der Plicht, J., 2013. INTCAL13 and MARINE13 radiocarbon age calibration curves 0-50,000 years cal BP. *Radiocarbon.* **55**, 1869-1887

Smith, M.A., 2006. Characterizing late Pleistocene and Holocene stone artefact assemblages from Puritjarra rock shelter: A long sequence from the Australian desert. *Records of the Australian Museum.* **58,** 371-410.

Ulm, S., 2002. Marine and estuarine reservoir effects in central Queensland, Australia: Determination of ΔR values. *Geoarchaeology.* **17(4),** 319-348.

Ulm, S., 2006. Australian marine reservoir effects: A guide to ΔR Values. *Aust. Archaeol.* 63, 57-60.

Williams, A.N., 2012. The use of summed radiocarbon probability distributions in archaeology: A review of methods. *J. of Archaeol. Sci.* **39,** 578-589.

Williams, A.N., 2013. A new population curve for prehistoric Australia. Proceedings of the Royal Society B. **280,** 20130486.

Williams, A.N., Ulm, S., 2016. Radiometric dates are a robust proxy for long-term demographic change: A comment on Attenbrow and Hiscock (2015). *Archaeol. in Ocean.* **51(3),** 216-217. doi:10.1002/arco.5095

Williams, A.N., Ulm, S., Cook, A.R., Langley, M.C., Collard, M., 2013. Human refugia in Australia during the Last Glacial Maximum and Terminal Pleistocene: A geospatial analysis of the 25-12ka Australian archaeological record. *J. of Archaeol. Sci*. **40,** 4612-4625.

Williams, A.N., Ulm, S. Turney, C.S.M., Rohde, D., White, G., 2015. Holocene demographic changes and the emergence of complex societies in prehistoric Australia. *PLoS ONE*. **10(6),** e0128661. doi:10.1371/journal.pone.0128661

Yokoyama, Y., De Deckker, P., Lambeck, K., Johnston, P., Fifield, L.K., 2001a. Sea-level at the Last Glacial Maximum: Evidence from northwestern Australia to constrain ice volumes for oxygen isotope stage 2. *Palaeogeography, Palaeoclimatology, Palaeoecology*. **165,** 218-297.

Yokoyama, Y., Esat, T.M., Lambeck, K., 2001b. Coupled climate and sea-level changes deduced from Huon Peninsula coral terraces of the last ice age. *Earth and Planetary Science Letters*. **193,** 579-587.